ELSEVIER

Journal of Quantitative Spectroscopy & Radiative Transfer 95 (2005) 429–467

Journal of Quantitative Spectroscopy & Radiative Transfer

www.elsevier.com/locate/jqsrt

The 2003 edition of the GEISA/IASI spectroscopic database

N. Jacquinet-Husson[a,*], N.A. Scott[a], A. Chédin[a], K. Garceran[a], R. Armante[a], A.A. Chursin[b], A. Barbe[c], M. Birk[d], L.R. Brown[e], C. Camy-Peyret[f], C. Claveau[f], C. Clerbaux[g,h], P.F. Coheur[h], V. Dana[f], L. Daumont[c], M.R. Debacker-Barilly[c], J.M. Flaud[i], A. Goldman[j], A. Hamdouni[c], M. Hess[d], D. Jacquemart[f], P. Köpke[k], J.Y. Mandin[f], S. Massie[l], S. Mikhailenko[b], V. Nemtchinov[m], A. Nikitin[b], D. Newnham[n,1], A. Perrin[i], V.I. Perevalov[b], L. Régalia-Jarlot[c], A. Rublev[o], F. Schreier[d], I. Schult[p], K.M. Smith[n], S.A. Tashkun[b], J.L. Teffo[f], R.A. Toth[e], Vl.G. Tyuterev[c], J. Vander Auwera[h], P. Varanasi[m], G. Wagner[d]

[a]*Laboratoire de Météorologie Dynamique/ Institut Pierre Simon Laplace, Ecole Polytechnique, Route Departmentale 36, 91128 Palaiseau, France*

[b]*Laboratory of Theoretical Spectroscopy, Institute of Atmospheric Optics, Russian Academy of Sciences, 634055 Tomsk, Russian Federation*

[c]*Groupe de Spectrométrie Moléculaire et Atmosphérique, Université de Reims-Champagne-Ardenne, 51062 Reims, France*

[d]*Remote Sensing Technology Institute, German Aerospace Center (DLR), Oberpfaffenhofen, D-82234 Wessling, Germany*

[e]*Jet Propulsion Laboratory, California Institute of Technology, Pasadena, CA 91109, USA*

[f]*Laboratoire de Physique Moléculaire et Applications, Université Pierre et Marie Curie, 75252 Paris, France*

[g]*Service d'Aéronomie/Institut Pierre Simon Laplace, Université Pierre et Marie Curie, 75252 Paris, France*

Abbreviation: AIRS: *A*dvanced*I*nfra*R*ed*S*ounder; *ARA*: *A*tmospheric *R*adiation *A*nalysis; *ATMOS* : *A*tmospheric *T*race *MO*lecule *S*pectroscopy; *4A*: *A*utomatized *A*tmospheric *A*bsorption *A*tlas; *CNES*: *C*entre *N*ational d'*E*tudes *S*patiales, France; *DLR: D*eutsches Zentrum für *L*uft und *R*aumfahrt: German Aerospace Center, Germany; *EPS*:*E*uropean *P*olar *S*ystem; *EUMETSAT*: *EU*ropean organization for the exploitation of *MET*eorological *SAT*ellites; *FITMAS*: *FIT M*olecular *A*bsorption *S*pectra code; *FTS: F*ourier *T*ransform *S*pectrometer; *GADS: G*lobal *A*erosol *D*ata *S*et; *GEISA*: *G*estion et *E*tude des *I*nformations *S*pectroscopiques *A*tmosphériques: Management and Study of Atmospheric Spectroscopic Information; *GIDSC*: *G*EISA/*I*ASI*D*atabase *S*cientific *C*ommittee; *GSMA*: *G*roupe de *S*pectrométrie *M*oléculaire et *A*tmosphérique; *HITRAN*: *HI*gh resolution *TRAN*smission spectroscopic database; *IASI*: *I*nfrared *A*tmospheric *S*ounder *I*nterferometer; *ISSWG*: *I*ASI *S*ounding *S*cience *W*orking *G*roup; *LMD*: *L*aboratoire de *M*étéorologie *D*ynamique; *LPMA*: *L*aboratoire de *P*hysique *M*oléculaire et *A*pplications; *METOP: MET*eorological *OP*erational Satellite; *OPAC: O*ptical *P*roperties of *A*erosols and *C*louds; *RAL*: *R*utherford *A*ppleton *L*aboratory; *rms*: *r*oot-*m*ean *s*quare; *S&MPO*: *S*pectroscopy *&* *M*olecular *P*roperties of *O*zone; *TIGR: T*hermodynami*c* *I*nitial *G*uess *R*etrieva*l*

*Corresponding author. Tel.: +33 1 69 33 48 02; fax: +33 1 69 33 37 58.

E-mail address: nicole.jacquinet@lmd.polytechnique.fr (N. Jacquinet-Husson).

0022-4073/$ - see front matter
doi:10.1016/j.jqsrt.2004.12.004

[h]Service de Chimie Quantique et Photophysique, Université Libre de Bruxelles, C.P. 160/09, B-1050 Brussels, Belgium
[i]Laboratoire Interuniversitaire des Systèmes Atmosphériques, Université Paris 12, 94010 Créteil, France
[j]Department of Physics, University of Denver, Denver, CO 80208, USA
[k]Meteorologisches Institut der Universität München, München, D-80333, Germany
[l]National Center for Atmospheric Research, Boulder, CO 80307, USA
[m]State University of New York at Stony Brook, Stony Brook, NY 11794, USA
[n]Rutherford Appleton Laboratory, Chilton, Didcot, Oxon, OX11 OQX, UK
[o]Institute of Molecular Physics at Russian Research Center Kurchatov Institute, Moscow 123183, Russian Federation
[p]Max-Planck-Institut für Meteorologie, D-20146 Hamburg, Germany

Received 23 July 2004; accepted 15 December 2004

Abstract

The content of the current (2003) version, *GEISA/IASI*-03, of the computer-accessible spectroscopic database, *GEISA/IASI*, is described. This "system" or database is comprised of three independent spectroscopic archives, which are (a) a database of individual spectral line parameters on 14 molecules, H_2O, CO_2, O_3, N_2O, CO, CH_4, O_2, NO, SO_2, NO_2, HNO_3, OCS, C_2H_2, N_2, and the related 51 isotopomers and isotopologues, representing 702,550 entries, in the spectral range 599–3001 cm^{-1}, (b) a database of spectral absorption cross-sections (6,572,329 entries related to six molecules, CFC-11, CFC-12, CFC-14, HCFC-22, N_2O_5, CCl_4), and a catalogue of microphysical and optical properties (mainly, the refractive indices) of atmospheric aerosols. The modifications and improvements, which have been implemented since the earlier editions of this database, in terms of content and management, have been explained in detail. *GEISA/IASI* has been created with the specific purpose of assessing the capability of measurement by the *IASI* instrument within the designated goals of *ISSWG* in the frame of the *CNES/EUMETSAT European Polar System* preparation.

All the archived data can be handled through a user-friendly associated management software, which is posted on the *ARA/LMD* group web site at http://ara.lmd.polytechnique.fr.

Keywords: *GEISA*; *GEISA/IASI*; Spectroscopic database; Atmospheric absorption; CFC's cross-sections; Atmospheric aerosols

1. Introduction

The new generation of, actual or planned, vertical sounding high-resolution infrared instruments, such as *AIRS* (http:www.airs.jpl.nasa.gov/) in the USA and *IASI* (http://earth-sciences.cnes.fr/IASI/) in Europe, will have improved vertical resolution and accuracy compared to the currently operating instruments. They will mainly be devoted to that aspect of operational meteorology, which is associated with numerical weather prediction, with the express purpose of providing improved information about the vertical atmospheric structure and surface properties. The performance of these second-generation vertical spatial sounders will highly depend on the

[1]Now at Terra View Limited, Cambridge CB4 0WS, UK

accuracy in the spectroscopic parameters of the optically active atmospheric gases, since such data constitute an essential input in the forward models that are used to interpret the recorded spectral radiance. Consequently, a strong demand exists for a highly comprehensive, well-validated, efficiently operational, and desirably interactive computer-based spectroscopic database. In order to meet demands such as these, the *ARA* group at *LMD* (see [1–4]) has been engaged during the past three decades in the development of *GEISA*. It is a computer-accessible database and was designed to facilitate accurate and fast, forward calculations of atmospheric radiative transfer using a line-by-line and (atmospheric) layer-by-layer approach. This effort has proven to be beneficial to the atmospheric scientific community participating in direct and inverse radiative transfer studies.

The *GEISA/IASI* database was derived from *GEISA* as described in Refs. [5,6]. It has been created for the purpose of assessing the capability of *IASI*, within the *ISSWG*, in the framework of the *EPS* preparation of *CNES/EUMETSAT*. The assessment will be done by simulating either high-resolution radiance spectra or experimental data, or both, as the situation demands. In order to bring about an improvement in our knowledge of spectroscopic parameters and to ensure the continuous upgrade and maintenance of *GEISA/IASI* during the 15 years of operation of the *IASI* instrument, *EUMETSAT* and *CNES* have created the *GIDSC*. *EUMETSAT* is planning to implement *GEISA/IASI* into the ground segment of *EPS*. There have been three versions of *GEISA/IASI* since its creation. They are all described in Refs. [6–8]. *GEISA/IASI*, in its current edition, is both an extract, from a more extensive *GEISA* database which has been devised to suit the needs of *IASI* or *AIRS* within the 599–3001 cm^{-1} spectral range and a continuing update of *GEISA-03* [8,9], which has a similar structure. It is comprised of the following three independent sub-databases devoted, respectively, to infrared spectral line parameters, infrared absorption cross-sections, microphysical and optical properties of atmospheric aerosols. A user can easily access and work with all of the archived data by using our user-friendly *GEISA*-associated management software (http://ara.lmd.polytechnique.fr).

2. Overview of the GEISA/IASI-03 sub-database on individual line transition spectroscopic parameters

This sub-database of *GEISA/IASI-03* has the necessary parameters of the well-resolved spectral lines of 14 molecules, whose 51 isotopomers/isotopologues[2] are included, and selected by the *GIDSC*. It contains 702,550 entries. The molecules involved are H_2O, CO_2, O_3, N_2O, CO, CH_4, O_2, NO, SO_2, NO_2, HNO_3, OCS, C_2H_2, and N_2. It has to be noticed that CH_3D (monodeuterated methane), independent molecule in *GEISA*, is considered as an isotopologue of CH_4 in *GEISA/IASI*.

The parameters of each spectral line or molecular vibrational–rotational transition are stored in the new "format standard" of *GEISA* and *GEISA/IASI-03* [8,9], with an extended number (from

[2]An isotopologue is a molecular twin, as it were, that differs from the original molecule in the isotopic composition (number of isotopic substitutions) only; for example, $^{13}CH_4$ and $^{12}CH_3D$ are isotopologues of $^{12}CH_4$. An isotopomer (a contraction of 'isotopic isomer'), on the other hand, has the same number of each of the isotopic atoms, but differing in their orientation within the molecular structure (giving rise to different spectra); for example, $^{16}O^{18}O^{16}O$ is an isotopomer of $^{16}O^{16}O^{18}O$ and so is $^{14}N^{15}NO$ of $^{15}N^{14}NO$.

16 to 30) of the selected line parameters with the associated error estimations. The file structure is presented in Table 1. Symbolic field names are in the first line, and the field lengths and format descriptors are in lines 2 and 3, respectively. The A–Q fields are similar to those described in Ref. [4], but with some extensions in the field lengths and differences in the description of the format. These differences are identified by a reminder of the former format in *italic*s. The description of each field is given at the bottom of the table.

As the continuum depends on the radiative transfer algorithm which has been used to fit the experimental measurements, it has been decided not to include the different published data on the continuum (i.e.: continuum of H_2O, O_2, N_2) in the *GEISA* database. We preferred, instead, to take these contributions into account in the line-by-line algorithms, such as *4A-2000* [10–12].

The details of the sub-database on line transition parameters are given in Table 2.

3. Details of the updates for individual line parameters in GEISA/IASI-03

The current edition of *GEISA/IASI* [8] is a significant update of the updates since the first edition in 1997 [6]. Among the data on the 14 selected molecular species, the data on 8 have been updated. In part (a) of Table 3, we present an overview of the updated data with the molecules listed in the first column, the whole extent of the spectral coverage in the second, the spectral intervals, in which modifications were made in the spectroscopic parameters, in the third column, and the associated references in the fourth column. In part (b) of Table 3, we list the molecules, whose data were not updated, in the first column, the extent of the spectral coverage in the second column, and in the third column, the reference to *GEISA-97* [4] where the spectroscopic parameters can be found.

We provide in the following sub-sections the details of the updated data by identifying the chemical formulae of the molecular species. A reminder of their *GEISA/IASI* identification code number is given as well.

3.1. H_2O (molecule 1)

Two different series of updated spectroscopic parameters of H_2O are catalogued. They stem from the measurements by Toth [13] and from the *EUMETSAT/RAL* archive [14]. Toth's data enter into the entire database, while the *EUMETSAT/RAL* data appear in a supplemental list. A choice cannot been made as to a final selection until the results of validation campaigns are used to study the respective accuracies in a detailed manner.

3.1.1. Toth's H_2O archive

The 500–2819 cm^{-1} region includes line parameters of water vapour computed using the measurements by Toth [15–25]. The listing of 10,755 transitions is for isotopologues: $H_2^{16}O$, $H_2^{17}O$, $H_2^{18}O$, $HD^{16}O$, $HD^{17}O$, and $HD^{18}O$. These species are coded as 161, 171, 181, 162, 172, and 182, respectively. The minimum value of the line strength value is set at 2.0×10^{-27} cm molecule^{-1} at 296 K. A detailed description of the compilation is given in part (a) of Table 4 and is divided into two parts. The left part of the table, related to the new data introduced into the database, lists the molecule and isotopologue codes in columns 1 and 2, respectively, the vibrational bands in

Table 1
Fields of the format for *GEISA/IASI-03* sub-database on line transition parameters

Field name	A	B	C	D	E	F	G	I	J	K	L	M	N	O	P	Q
Field length	12	11	6	10	36	4	3	3	1	2	1	10	5	8	3	6
Fortran descriptor	F12.6 (*F10.6*)	D11.4 (*D10.3*)	F6.4 (*F5.3*)	F10.4 (*F10.3*)	A36	F4.2	I3	I3	A1 (*A3*)	I2	I1	E10.3	F5.4	F8.6	I3	I6

	R	*A′*	*B′*	*C′*	*F′*	*O′*	*R′*	*N′*	*S*	*S′*	*T*	*T′*	*U*	*U′*
Fields length	6	10	11	6	4	8	6	5	4	4	8	8	4	4
Fortran descriptor	F6.4	F10.6	D11.4	F6.4	F4.2	F8.6	F6.4	F5.4	F4.2	F4.2	F8.6	F8.6	F4.2	F4.2

Fields A–Q previously in GEISA/IASI-97 [6]

A: Wavenumber (cm^{-1}) of the line.
B: Intensity of the line ($cm\,molecule^{-1}$) at 296 K.
C: Lorentzian air collision half-width (HWHM) ($cm^{-1}atm^{-1}$) at 296 K.
D: Energy of the lower transition level (cm^{-1}).
E: Transition quantum identifications for the lower and upper states of the transition.
F: Temperature dependence coefficient *n* of the Lorentzian air collision half-width.
G: Identification code for isotope as in *GEISA*.
I: Identification code for molecule as in *GEISA*.
J: Internal GEISA code for the data identification.
K: Molecule number as in *HITRAN*.
L: Isotope number (1 = most abundant. 2 = second, .. etc.) as in *HITRAN* [27].
M: Transition probability (in $debye^2$).
N: Self-broadening pressure half-width (HWHM) ($cm^{-1}\,atm^{-1}$) at 296 K (for water).
O: Air pressure shift of the line transition ($cm^{-1}\,atm^{-1}$) at 296 K.
P: Accuracy indices for wavenumber, intensity and half-width.
Q: Indices for lookup of references for wavenumber, intensity and half-width.

Fields R–U′ new for GEISA/IASI-03 [8]

R: Temperature dependence coefficient *n* of the air pressure shift.
A′: Estimated accuracy (cm^{-1}) on the line position.
B′: Estimated accuracy on the intensity of the line in ($cm^{-1}/(molecule\,cm^{-2})$).
C′: Estimated accuracy on the Lorentzian air collision half-width (HWHM) ($cm^{-1}\,atm^{-1}$).
F′: Estimated accuracy on the temperature dependence coefficient *n* of the Lorentzian air collision half-width.
O′:Estimated accuracy on the air pressure shift of the line transition ($cm^{-1}\,atm^{-1}$) at 296 K.
R′: Estimated accuracy on the temperature dependence coefficient *n* of the air pressure shift.
N′: Estimated accuracy on the self broadened (HWHM) ($cm^{-1}\,atm^{-1}$) at 296 K (for water).
S: Temperature dependence coefficient *n* of the self-broadening half-width (for water).
S′: Estimated accuracy on the temperature dependence coefficient *n* of the self-broadening half-width (for water).
T: Self pressure shift of the line transition ($cm^{-1}\,atm^{-1}$) at 296 K (for water).
T′: Estimated accuracy on the self pressure shift of the line transition ($cm^{-1}\,atm^{-1}$) at 296 K (for water).
U: Temperature dependence coefficient *n* of the self-pressure shift (for water).
U′: Estimated accuracy on the temperature dependence coefficient *n* of the self-pressure shift (for water).

Table 2
GEISA/IASI-03 sub-database on line transition parameters detailed content

Molecule	# lines	Intensity average (cm molecule^{-1})	Alpha[a] average (cm^{-}atm^{-1})	Isotope code	# lines	Minimum wavenumber (cm^{-1})	Maximum wavenumber (cm^{-1})	Minimum intensity (cm molecule^{-1})	Maximum intensity (cm molecule^{-1})
H_2O (Toth)	13,278	8.113×10^{-22}	0.0655	161	5219	599.681	2999.854	9.010×10^{-28}	2.990×10^{-19}
				162	4584	604.366	2999.340	1.000×10^{-27}	2.510×10^{-23}
				171	1203	599.702	2999.532	1.490×10^{-27}	1.210×10^{-22}
				181	1659	604.933	3000.882	2.030×10^{-27}	6.050×10^{-22}
				182	438	1173.772	1684.226	2.030×10^{-27}	5.080×10^{-26}
				172	175	1234.235	1598.765	2.030×10^{-27}	9.320×10^{-27}
H_2O (RAL)	12,146	8.767×10^{-22}	0.0665	161	4600	599.671	2999.854	9.010×10^{-28}	2.920×10^{-19}
				162	4586	607.371	2999.340	1.000×10^{-27}	2.670×10^{-23}
				171	1198	599.704	2999.532	1.490×10^{-27}	1.120×10^{-22}
				181	1466	606.145	3000.882	2.030×10^{-27}	6.160×10^{-22}
				182	281	1173.772	1607.611	2.060×10^{-27}	7.940×10^{-26}
				172	15	1234.235	1293.770	2.060×10^{-27}	5.120×10^{-27}
CO_2	50,840	2.165×10^{-21}	0.0711	626	18,811	599.222	2488.222	3.440×10^{-39}	3.530×10^{-18}
				636	7576	599.026	2395.279	1.820×10^{-39}	3.750×10^{-20}
				628	12,106	599.007	2826.650	1.390×10^{-36}	6.840×10^{-21}
				627	7591	599.183	2806.199	1.000×10^{-27}	1.250×10^{-21}
				638	1833	599.165	2605.481	3.700×10^{-27}	7.230×10^{-23}
				637	1346	599.008	2314.307	3.710×10^{-27}	1.360×10^{-23}
				828	994	615.974	2350.898	1.760×10^{-40}	1.310×10^{-23}
				728	288	626.438	2358.226	3.870×10^{-27}	2.500×10^{-24}
				838	295	2115.685	2276.481	4.870×10^{-42}	1.760×10^{-25}
O_3	195,102	8.814×10^{-23}	0.0694	666	152,546	599.043	3000.984	9.712×10^{-27}	4.060×10^{-20}
				668	14,350	599.001	1177.493	9.154×10^{-26}	7.760×10^{-23}
				686	19,880	605.293	2259.896	9.970×10^{-29}	7.560×10^{-23}
				667	5515	599.123	820.380	3.423×10^{-27}	5.356×10^{-25}
				676	2811	599.382	822.795	3.394×10^{-27}	5.827×10^{-25}

N_2O	18,966	3.628×10^{-21}	0.0744	446	13,301	599.027	2836.125	1.280×10^{-28}	1.000×10^{-18}
				456	1623	599.826	2595.681	1.220×10^{-25}	3.670×10^{-21}
				546	1655	599.129	2585.207	1.210×10^{-25}	3.600×10^{-21}
				448	1596	599.321	2543.215	1.230×10^{-25}	2.050×10^{-21}
				447	791	599.420	2560.588	6.180×10^{-26}	4.150×10^{-22}
CO	3674	2.748×10^{-21}	0.0467	26	1499	1523.979	2316.048	6.840×10^{-70}	4.460×10^{-19}
				36	1263	1544.497	2259.947	1.880×10^{-65}	4.690×10^{-21}
				27	229	1831.283	2278.722	1.250×10^{-36}	1.600×10^{-22}
				28	240	1797.966	2254.309	1.250×10^{-36}	8.320×10^{-22}
				37	217	1807.871	2221.114	1.030×10^{-36}	1.680×10^{-24}
				38	226	1779.750	2196.287	1.500×10^{-36}	8.700×10^{-24}
CH_4	121,281	6.891×10^{-23}	0.0498	211	68,777	922.651	3000.998	1.000×10^{-27}	1.200×10^{-19}
				311	22,688	998.884	3000.999	9.490×10^{-28}	1.340×10^{-21}
				212	29,816	855.753	3000.997	6.160×10^{-29}	3.660×10^{-23}
O_2	435	2.191×10^{-29}	0.0466	66	435	1366.105	1717.236	1.100×10^{-35}	1.490×10^{-28}
NO	29,608	1.562×10^{-22}	0.0522	46	28,230	599.089	3000.718	1.510×10^{-85}	2.320×10^{-20}
				48	679	1601.909	2038.846	4.190×10^{-28}	1.390×10^{-22}
				56	699	1609.585	2060.462	4.430×10^{-28}	2.550×10^{-22}
SO_2	22,301	1.566×10^{-21}	0.1132	626	22,014	599.173	2787.861	5.000×10^{-26}	6.090×10^{-20}
				646	287	2463.470	2496.088	9.740×10^{-24}	3.430×10^{-23}
NO_2	71,687	8.646×10^{-22}	0.0672	646	71,687	599.083	2992.323	9.470×10^{-26}	1.300×10^{-19}
HNO_3	152,586	6.928×10^{-22}	0.1101	146	152,586	599.003	1769.982	1.050×10^{-25}	3.020×10^{-20}
OCS	19,768	5.801×10^{-21}	0.0898	622	11,005	814.581	2962.986	1.010×10^{-23}	1.220×10^{-18}
				624	3810	813.860	2926.274	1.010×10^{-23}	4.720×10^{-20}
				632	2048	825.716	2880.701	1.010×10^{-23}	1.200×10^{-20}
				623	1593	825.659	2930.386	1.020×10^{-23}	8.430×10^{-21}

Table 2 (*continued*)

Molecule	# lines	Intensity average (cm molecule^{-1})	Alpha[a] average (cm^{-}atm^{-1})	Isotope code	# lines	Minimum wavenumber (cm^{-1})	Maximum wavenumber (cm^{-1})	Minimum intensity (cm molecule^{-1})	Maximum intensity (cm molecule^{-1})
				822	955	818.098	2875.829	1.010×10^{-23}	2.090×10^{-21}
				634	357	1972.188	2032.039	1.010×10^{-23}	5.240×10^{-22}
C_2H_2	2904	1.114×10^{-20}	0.0701	221	2754	604.774	2254.963	9.490×10^{-27}	1.190×10^{-18}
				231	150	613.536	843.872	3.820×10^{-26}	1.580×10^{-20}
N_2	120	5.601×10^{-29}	0.0419	44	120	1992.628	2625.497	2.190×10^{-34}	3.420×10^{-28}

[a] Lorentzian air collision half-width at 296 K.

Column 1: Molecular species archived in *GEISA/IASI-03*.
For each molecular species listed in column 1:
Column 2: Total number of lines.
Column 3: Intensity average (cm molecule^{-1} at 296 K).
Column 4: Mean half-width at half maximum (cm^{-1} atm^{-1}).
Column 5: Isotope identification codes [4].

For each isotope listed in column 5:
Column 6: Number of lines.
Column 7: Transition minimum wavenumber (cm^{-1}).
Column 8: Transition maximum wavenumber (cm^{-1}).
Column 9: Lines minimum intensity (cm molecule^{-1} at 296 K).
Column 10: Lines maximum intensity (cm molecule^{-1} at 296 K).

Table 3
GEISA/IASI-03 sub-database on line transition parameters: overview of content and data sources

(a) *Updated molecules*

Molecule	Spectral intervals (cm^{-1})	Modified spectral intervals (cm^{-1})	Refs.
H_2O (Toth)	599.681–3000.882	599.681–2819.848	[13,15–25]
H_2O (RAL)	599.670–3000.882	700.032–1299.980	[14]
CO_2	599.007–2826.650	599.0070–2826.650	[28–33]
O_3	599.001–3000.984	600.1793–1272.422 1311.101–1525.957 1617.059–2536.503 2597.442–3001	[34–55]
N_2O	599.027–2836.125	872.399–1243.755	[56–60]
CH_4	855.753–3000.999	922.651–3001	[61–77]
NO	599.089–3000.718	1487.366–2188.448	[78–80]
NO_2	599.083–2992.323	2719.056–2992.323	[81–86]
C_2H_2	604.774–2254.963	604.774–2254.963	[87–97]

(b) *Non-updated molecules*:

Molecule	Spectral intervals (cm^{-1})	Ref.
CO	1523.979–2316.048	
O_2	1366.105–1717.236	
SO_2	599.173–2787.861	*GEISA* 97 [4]
HNO_3	599.003–1769.982	
OCS	813.860–2962.986	
N_2	1992.628–2625.497	

column 3. For each band, the number of lines, the minimum and maximum wavenumbers of the rotational transitions (cm^{-1}), the minimum and maximum values of the line strengths (cm molecule^{-1} at 296 K), and the maximum J value, are listed in columns 4–9, respectively. The total number of updated entries for H_2O is given at the bottom of the table. In addition, the right part of the table gives, in columns 10–15, the total number of lines, the minimum and maximum wavenumber (cm^{-1}), the minimum and maximum line strength (in cm molecule^{-1} at 296 K), and the maximum J value for the measured transitions from which the compiled data were derived. The entire list includes air- and self-broadened half-width as well as pressure-induced frequency shifts derived from the studies by Toth [21–25]. The values of the exponent n, which is used to depict the temperature dependence of these parameters, taken from the prior versions of *GEISA* [4,5] and *HITRAN* [26,27], were inserted for a handful of individual transitions. For unmeasured transitions, the exponents were set to values ranging from 0.35 to 0.80 for values of the rotational quantum number J ranging from 1 to 9.

Table 4
Description of updated H_2O content in *GEISA/IASI*-03 sub-database on line transition parameters

(a) *Toth's update*

				Total *GEISA/IASI*-03 Toth's transitions						Toth's measured transitions					
Molecule code	Isotope code	Band[a]		# lines	Minimum wavenumber (cm^{-1})	Maximum wavenumber (cm^{-1})	Minimum intensity (cm molecule^{-1})	Maximum intensity (cm molecule^{-1})	J_{max}	# lines	Minimum wavenumber (cm^{-1})	Maximum wavenumber (cm^{-1})	Minimum intensity (cm molecule^{-1})	Maximum intensity (cm molecule^{-1})	J_{max}
1	161	000	000	483	599.6811	1743.9773	2.05×10^{-27}	2.32×10^{-21}	21	307	590.3311	1285.6899	6.74×10^{-27}	3.85×10^{-21}	19
1	161	010	010	120	601.5921	1029.4600	2.09×10^{-27}	2.29×10^{-27}	18	49	590.6003	851.2487	1.90×10^{-26}	3.27×10^{-24}	15
1	161	010	000	1903	701.9643	2819.8482	2.02×10^{-27}	2.99×10^{-19}	21	1282	783.2109	2582.6184	6.94×10^{-27}	2.98×10^{-19}	20
1	161	020	010	872	877.3133	2628.5776	2.05×10^{-27}	2.77×10^{-22}	16	505	995.9774	2276.5521	5.00×10^{-27}	2.75×10^{-22}	14
1	161	100	010	532	1221.4101	2611.6646	2.02×10^{-27}	3.90×10^{-24}	14	255	1247.8814	2423.0689	6.09×10^{-27}	3.90×10^{-24}	12
1	161	001	010	484	1298.1172	2716.1280	2.08×10^{-27}	9.40×10^{-24}	14	229	1298.1172	2571.9108	6.29×10^{-27}	9.48×10^{-24}	13
1	161	030	020	382	1122.1609	2698.5661	2.03×10^{-27}	2.24×10^{-25}	11	33	1293.6548	1841.5484	1.78×10^{-26}	2.20×10^{-25}	6
1	181	000	000	137	604.9330	1107.8835	2.03×10^{-27}	4.60×10^{-24}	17	76	595.5295	943.9840	1.57×10^{-26}	4.84×10^{-24}	16
1	181	010	010	6	608.2360	674.0171	2.05×10^{-27}	7.54×10^{-27}	12						
1	181	010	000	1031	893.5514	2310.5115	2.03×10^{-27}	6.05×10^{-22}	18	731	1009.5539	2219.1683	8.31×10^{-27}	6.13×10^{-22}	17
1	181	020	010	303	1203.3157	2014.5525	2.03×10^{-27}	5.85×10^{-25}	12	167	1284.7791	1934.9395	3.60×10^{-27}	6.13×10^{-25}	11
1	181	100	010	63	1807.7875	2248.8805	2.06×10^{-27}	1.05×10^{-26}	8						
1	181	001	010	59	2004.6187	2305.8356	2.07×10^{-27}	1.96×10^{-26}	8						
1	171	000	000	88	599.7018	976.2445	2.06×10^{-27}	8.35×10^{-25}	15	31	598.9986	797.3165	1.21×10^{-26}	9.07×10^{-25}	14
1	171	010	000	841	1007.7228	2260.6045	2.03×10^{-27}	1.21×10^{-22}	17	660	1063.7848	2224.1543	1.81×10^{-27}	1.12×10^{-22}	17
1	171	020	010	190	1270.3184	1939.9008	2.06×10^{-27}	1.05×10^{-25}	11	109	1314.1474	1939.9008	2.29×10^{-27}	9.68×10^{-26}	9
1	162	000	000	78	604.3662	834.7326	2.02×10^{-27}	7.10×10^{-26}	17	56	651.0778	834.7326	1.91×10^{-27}	7.02×10^{-26}	16
1	162	010	000	1710	917.3648	1921.2779	2.02×10^{-27}	2.51×10^{-23}	20	1413	917.3648	1921.2779	1.48×10^{-27}	2.52×10^{-23}	19
1	162	020	010	435	1145.2243	1695.0543	2.02×10^{-27}	6.49×10^{-26}	13	325	1155.8371	1695.0543	1.94×10^{-27}	6.70×10^{-26}	13
1	162	100	010	33	1230.7725	1574.1042	2.02×10^{-27}	3.92×10^{-27}	7	24	1230.7725	1574.1042	1.88×10^{-27}	3.81×10^{-27}	6
1	182	010	000	438	1173.7720	1684.2263	2.03×10^{-27}	5.08×10^{-26}	13	410	1173.7720	1684.2263	1.95×10^{-27}	5.16×10^{-26}	13
1	172	010	000	175	1234.2347	1598.7655	2.03×10^{-27}	9.32×10^{-27}	10	137	1234.2347	1598.7655	1.81×10^{-27}	9.20×10^{-27}	10

Total number of updated lines: 10,363

(b) *RAL update*

Total *GEISA/IASI*-03 *RAL* Transitions									
Molecule code	Isotope code	Band[a]		# lines	Minimum wavenumber (cm^{-1})	Maximum wavenumber (cm^{-1})	Minimum intensity ($cm\,molecule^{-1}$)	Maximum intensity ($cm\,molecule^{-1}$)	J_{max}
1	161	001	020	40	700.0318	913.0041	1.10×10^{-27}	4.92×10^{-26}	11
1	162	000	000	42	700.5583	834.7326	2.02×10^{-27}	1.96×10^{-26}	16
1	181	000	000	90	701.6535	1107.8835	2.03×10^{-27}	1.16×10^{-24}	17
1	161	010	000	381	701.9643	1299.7075	1.03×10^{-27}	1.91×10^{-21}	20
1	171	000	000	49	702.2621	976.2445	2.18×10^{-27}	2.09×10^{-25}	15
1	161	000	000	346	703.3173	1299.2984	1.07×10^{-27}	5.67×10^{-22}	20
1	161	100	020	4	707.4805	829.0096	1.46×10^{-27}	2.03×10^{-27}	7
1	161	010	010	103	708.2294	1133.9751	1.00×10^{-27}	4.11×10^{-25}	17
1	161	020	010	161	819.7765	1299.7354	1.01×10^{-27}	7.83×10^{-24}	17
1	181	010	000	130	893.5514	1298.1596	2.03×10^{-27}	3.84×10^{-24}	17
1	162	010	000	514	917.3648	1299.9799	2.02×10^{-27}	1.38×10^{-23}	18
1	171	010	000	80	1007.7228	1294.7188	2.05×10^{-27}	7.18×10^{-25}	15
1	161	030	020	34	1122.1609	1299.0650	2.11×10^{-27}	3.00×10^{-26}	13
1	162	020	010	125	1145.2243	1299.3177	2.05×10^{-27}	3.41×10^{-26}	11
1	182	010	000	81	1173.7720	1299.8655	2.06×10^{-27}	2.78×10^{-26}	11
1	181	020	010	15	1203.3157	1293.6796	2.09×10^{-27}	1.80×10^{-26}	8
1	161	100	010	5	1221.4100	1292.0303	3.40×10^{-27}	8.69×10^{-26}	10
1	162	100	010	13	1230.7725	1289.1217	2.08×10^{-27}	3.61×10^{-27}	6
1	172	010	000	15	1234.2348	1293.7703	2.06×10^{-27}	5.12×10^{-27}	8
1	171	020	010	3	1270.3185	1290.5311	2.27×10^{-27}	3.24×10^{-27}	7
1	161	001	010	1	1298.1170	1298.1170	1.11×10^{-25}	1.11×10^{-25}	7
Total number of updated lines: 2232									

[a]Upper level of the transition to the left and lower level to the right parts of the column.

3.1.2. *EUMETSAT/RAL archive*

In the framework of the *EUMETSAT* contract entitled, "Support Study on Water Vapour for *IASI*" [14], infrared line parameters of water vapour, with the associated uncertainties in their values, have been determined in the 700–1300 cm^{-1} spectral region from ten air-broadened, high-resolution, long-path, variable-temperature experimental transmittance spectra recorded at the molecular spectroscopy facility of *RAL* as part of the *VIRTEM*[3] project. Individual empirical values of line positions (cm^{-1}), air-pressure shifts ($cm^{-1}\,atm^{-1}$), intensities ($cm\,molecule^{-1}$ at 296 K), and air-broadened widths ($cm^{-1}\,atm^{-1}$) have been determined using standard, well-established computer-based non-linear least-squares techniques in which line-by-line spectra are calculated, compared with the observed spectra, and the line parameter values adjusted iteratively until the required degree of iteration of the fit is achieved. These experimental data have been fitted to the most recent theoretical models (L Coudert, J-M Hartman and J-M Flaud, private communication). A list of line positions, line intensities and line widths has been generated. Uncertainties have been evaluated from a combination of the experimental errors, statistical errors in the line-fitting routine, and the standard deviation of values determined from different transmittance spectra and merged together. The ability of the final linelist (referred to as *EUMETSAT/RAL*) to simulate the observed spectra has been tested, and any related problems have been identified and resolved. The content of the *EUMETSAT/RAL* H_2O archive is given in part (b) of Table 4, following the same presentation as part (a), in columns 1–9.

3.2. *CO_2 (molecule 2)*

Previously catalogued parameters of spectral lines belonging to the four most abundant isotopologues, $^{12}C^{16}O_2$, $^{13}C^{16}O_2$, $^{16}O^{12}C^{18}O$ and $^{16}O^{12}C^{17}O$, have been updated with 44,748 new entries covering the 599.007–2826.650 cm^{-1} spectral range. The line positions and line intensities of these transitions were calculated by Tashkun et al. [28–31] using the theory of effective operators developed for linear molecules by Teffo et al. [32,33].

The updating of the database includes several stages. Firstly, phenomenological models of effective Hamiltonian and effective dipole moment operators are built. Then the parameters of these models are fitted to the observed data (line positions, line intensities, correspondingly). Finally, a dedicated version of the database is generated from the fitted parameters by calculation of all possible lines, which have intensities above the given cut-off at the reference temperature.

The phenomenological model of an effective Hamiltonian (H^{eff}) is a linear combination of all symmetry allowed elementary rovibrational operators written up to a given order of the perturbation theory. The numerical coefficients of the combination are considered as adjustable parameters. The optimal values of the parameters are determined from a fitting of the model to a set of observed line positions. The model enables one to perform rotational and vibrational extrapolations, but it does not provide isotopic extrapolation. Each species has a specific H^{eff}. The effective Hamiltonian has been developed using the assumption of polyad structure of the vibrational energy levels, which arises due to the approximate relations between harmonic

[3] *V*alidation of *I*ASI *R*adiative *T*ransfer: *E*xperiments and *M*odelling EC contract Number ENV4-CT-0738.

frequencies of the molecule:

$$\omega_1 \approx 2\omega_2, \quad \omega_3 \approx 3\omega_2.$$

Each polyad is made up of the vibrational base states, whose respective quantum numbers fulfill the relation:

$$P = 2V_1 + V_2 + 3V_3,$$

where V_1, V_2, and V_3 denote normal modes of vibration. Thus, the polyads can be labeled with the value of the integer P, which can be considered as the quantum number identifying the polyad. The other good quantum numbers are the rotational quantum number J, and the parity of the level is designated by the symbol C, which is 1 or 2. It corresponds to the usual e or f labels, respectively. Inside a P, J, C block, the only way to unambiguously assign the ro-vibrational energy levels is to use their ranking index N, starting from the lowest. Up to now, this approach was successfully applied to $^{12}C^{16}O_2$, $^{13}C^{16}O_2$, $^{16}O^{12}C^{18}O$ and $^{16}O^{12}C^{17}O$ isotopologues of CO_2. More details of the effective Hamiltonian are given in Tashkun et al. [28].

For each transition listed in the database, the P, C, N numbers of the upper and lower levels have been added between the general vibrational index and the line identifier. Except for very few high-energy levels affected by strong l-type interactions, there is a one to one correspondence between the P, C, N labelling and the usual (V_1, V_2, l_2, V_3, r) labelling currently used for CO_2 in *GEISA* and *HITRAN*.

The model of the effective dipole moment operator is based on the same principles as the model of the effective Hamiltonian. Details of the effective dipole moment operator can be found in Tashkun et al. [29], where this model has been applied to global fittings of observed line intensities of $^{12}C^{16}O_2$. The model uses a serial approach. All bands are divided into series, which do not cross over. Each series is determined by the value of $\Delta P = P' - P$, where, P' and P are the quantum numbers of the upper and lower states, respectively, of the polyads. Each series has its own set of parameters of the effective dipole moment, which can be fitted to the corresponding observed data separately.

It is worth noting that 12,833 lines, which are absent in the previous version of the database, have been added. The air- and self-broadened half-widths, the coefficients of temperature dependence of these parameters, and air-induced pressure shifts of these transitions were taken from Refs. [26,27].

Confidence intervals of 3sigma are assumed for calculated accuracies of line positions and intensities.

3.3. O_3 (molecule 3)

The updates reported here are in five spectral regions.

3.3.1. Spectral region 600–1232 cm^{-1}

Retrieval of spectral line parameters from measurements: In the temperature range 200–300 K, a total of 16 spectra of ozone, and of ozone–nitrogen and ozone–oxygen mixtures, with the partial pressures of ozone ranging from 0.2 to 9 hPa, and the pressures of the broadening gases ranging from 20 to 55 hPa, were recorded at *DLR* with a high-resolution *FTS* [34]. The measurements are

on the lines of the three fundamental bands, which are situated in the 600–1232 cm^{-1} spectral region. Special attention was paid to avoid, as well as to assess, the various sources of systematic errors, which can stem from inhomogeneity in the temperature at which the measurement was reported, distortion of the observed spectra by instrumental line shape that was inherent, non-linearity in the signal sensed by detector used, and the chemical decomposition of the molecule itself during the course of the measurement. The spectra were analysed by employing the *FITMAS* code [34], which uses fully analytical Jacobians and allows to select line parameters to be fitted individually for each line. More details concerning the experimental and data reduction procedures are given by Wagner et al. [35].

Line positions: The line positions were fitted with a model [36], in which the various resonances affecting the ozone energy levels were taken into account. An improvement was achieved for the Hamiltonian constants (vibrational energies, rotational, centrifugal distorsion and coupling constants) in the (1 0 0), (0 1 0), (0 0 1), (1 1 0), and (0 1 1) states of $^{16}O_3$ using a fitting routine that combined the new data with existing infrared and microwave data. Constants for the states (0 2 0), (1 2 0), (0 2 1), (2 0 0), (1 0 1), (0 0 2) of $^{16}O_3$, as well as for the (1 0 0) and (0 0 1) of $^{16}O^{18}O^{16}O$ and $^{16}O^{16}O^{18}O$, were taken from Refs. [37–39] and the references contained therein.

Line intensities: Vibrational transition moments together with their rotational corrections were determined by fitting the measured intensities of the fundamental bands of $^{16}O_3$, whereas the harmonic approximation was used for the *hot* bands, $2\nu_2-\nu_2$, $2\nu_1-\nu_1$, $2\nu_3-\nu_3$, $\nu_2+\nu_3-\nu_2$, $\nu_1+\nu_2-\nu_2$, $\nu_1+\nu_3-\nu_1$, and $2\nu_2+\nu_1-2\nu_2$. In the case of the two bands, $2\nu_1-\nu_3$ and $2\nu_2+\nu_3-2\nu_2$, only the vibrational transition moments could be determined. For the isotopomers $^{16}O^{18}O^{16}O$ and $^{16}O^{16}O^{18}O$, however, the transition moments need to be improved. Finally, new line positions and line strengths were generated [35] for lines with $J\leqslant 90$, $K_a\leqslant 30$ and the line strength $\geqslant 10^{-25}$ cm molecule^{-1} at 296 K.

Air-broadened half-widths of spectral lines: The measured half-width of a so-called Lorentz line representing a given transition is entered into a least-squares-fitting routine to yield a set of air-broadened half-widths and a set of values of the exponent, n, in terms of which the variation of the half-width upon temperature is expressed. In this way, 500, 400, 1100 air-broadened half-widths and 250, 200, 500 temperature exponents were obtained for the ν_1, ν_2, ν_3 bands, respectively, for nitrogen and oxygen broadening. To improve the statistical uncertainty and to get interpolated values for lines for which measurements were not possible due to insufficient signal-to-noise ratio or blending, the measured broadening parameters were fitted to polynomials in the quantum number m (J'' for P and Q branches, $J''+1$ for R branches). Data for sub-bands were fitted together whenever no systematic difference between their parameters could be observed, thus further improving statistical uncertainty. The same was done for P- and R-branch lines and for ν_1 and ν_2 which have the same selection rules (B-type bands). Temperature exponents were treated in a similar way. The fitted polynomial coefficients were then used to calculate pressure-broadening parameters and temperature exponents within a meaningful range of m values. The air-broadening parameters were finally calculated as weighted averages of the nitrogen- and oxygen-broadening parameters. More details can be found in Ref. [35].

The list includes not only the three fundamental bands of $^{16}O_3$ but also lines of $^{16}O^{18}O^{16}O$ and $^{16}O^{16}O^{18}O$, which are observable at high spectral resolution in the ν_3 region over long atmospheric paths. It provides one with better line positions. As far as the line intensities are concerned, the average ratios of the new integrated intensities for the ν_2, ν_1 and ν_3 bands of $^{16}O_3$, when compared

to the previous values (see Refs. [4,40]), are 0.978, 0.965 and 0.973, respectively. These results are consistent with the conclusions of a recent paper [41], which compared the measurements of different groups [35,42–44], and derived ratios of 0.958 and 0.966 for the v_1 and v_3 bands, respectively. As a consequence, intensities of other bands in the 10 μm region, as well as of all lines in the shorter wavelength regions currently in *GEISA/IASI*, have been reduced by a similar scale factor of about 1.04, to maintain consistency throughout the infrared spectral region in the database. Also, it is worth noticing that the air-broadening parameters and temperature exponents for the main isotopomer fundamental bands were replaced by the polynomial values determined within the meaningful range of m values; all other parameters were left unchanged.

3.3.2. Spectral region 1300–1500 cm^{-1} ($^{16}O_3$)

The main bands observable in this region correspond to $2v_2$ with its associated hot band $3v_2 - v_2$, as well as the difference band $v_1 + v_3 - v_2$. This region was analysed from *ATMOS* [45] stratospheric solar occultation spectra recorded during the Spacelab 3 mission [46], leading to assignments up to $J = 37$ and $K_a = 8$ for the $2v_2$ band.

Barbe et al. [47], at *GSMA*, analysed this spectral range using laboratory *FTS* spectra with a long absorption path, recorded with a signal-to-noise ratio of 500. The J and K_a observed transitions increase to 57 and 16, respectively, leading obviously to improvements of the Hamiltonian parameters: 76.5% of the levels are now reproduced with an accuracy better than $0.6 \times 10^{-3}\,cm^{-1}$. A fit of 268 line intensities provides three transition moment parameters, and a complete calculation for $2v_2$ is performed up to $J = 65$, $K_a = 20$, with a cut-off of $2 \times 10^{-26}\,cm\,molecule^{-1}$ at 296 K. In addition, the weak hot band $3v_2 - v_2$ has been observed [47], leading to the Hamiltonian parameter of the (0 3 0) state. For that band, 17 measured line intensities have been fitted, using two statistically defined transition moment parameters. These two sets of parameters (Hamiltonian and transition moment) provide full calculation of the $3v_2 - v_2$ hot band for $J \leqslant 53$ and $K_a \leqslant 12$. The integrated band intensity is $S_V(3v_2 - v_2) = 2.9 \times 10^{-23}\,cm\,molecule^{-1}$ at 296 K, with a cut-off of $3 \times 10^{-26}\,cm\,molecule^{-1}$.

The two difference bands in this region, $v_1 + v_3 - v_2$ and $2v_3 - v_2$, have been observed also from laboratory spectra [48]. The dipole moment parameters have been derived from the experimental line intensities of these bands. A final list of transitions has been generated with an intensity cut-off of $2 \times 10^{-26}\,cm\,molecule^{-1}$ at 296 K. The integrated band intensities are $S_V(v_1 + v_3 - v_2) = 9.7 \times 10^{-22}$ and $S_V(2v_3 - v_2) = 1.1 \times 10^{-22}\,cm\,molecule^{-1}$ at 296 K, for the $v_1 + v_3 - v_2$ and $2v_3 - v_2$ bands, respectively.

The complete calculation of all this spectral range is included in the *S&MPO* database (see related web sites at: http://ozone.univ-reims.fr and http://ozone.iao.ru and references therein).

3.3.3. Spectral range 1820–2260 cm^{-1} ($^{16}O^{18}O^{16}O$)

A total of 1456 transitions of the $2v_3$, $v_1 + v_3$, and $2v_1$ interacting bands of the $^{16}O^{18}O^{16}O$ ozone isotopomer have been observed recently by De Backer-Barilly et al. [49], with the same *FTS* as in the above 1300–1500 cm^{-1} spectral region. Lines of the $2v_3$ and $2v_1$ bands are first observations. The analysis leads to the determination of the Hamiltonian parameters for the three upper states, those of the ground state being fixed [50]. The r.m.s. deviation of the line position fit is $0.77 \times 10^{-3}\,cm^{-1}$. Transition moment parameters for the three bands are determined from measured

relative intensities and allow to calculate a full line list (14,698 entries), performed with an intensity cut-off of 3×10^{-26} cm molecule^{-1}, up to $J_{max} = 65$, $K_{a\ max} = 20$ and a partition function Z (296 K) = 3599.

3.3.4. Spectral range 2600–2900 cm^{-1} ($^{16}O_3$)

This region, which contains the "triad 1", $v_2 + 2v_3$, $v_1 + v_2 + v_3$ and $2v_1 + v_2$, has been reinvestigated recently by Mikhailenko et al. [51] by introducing new rovibrational resonances. They studied the resonance between the nine interacting states, (0 1 2), (1 1 1), (0 4 0), (2 1 0), (0 0 3), (1 0 2), (2 1 0), (1 3 0) and (3 0 0). A total of 4520 energy levels were derived from observed transitions, and a suitable model had led to the reproduction of 3492, i.e., 77.3% of the total number, of levels with an uncertainty that was less than 0.7×10^{-3} cm^{-1} (see *S&MPO* database web sites and Ref. [51] for details).

The intensities of 2580 lines in seven of the strongest bands have led to transition moments with an r.m.s of 6.9% on the fitting of the intensities. Derived Hamiltonian and transition moment parameters allow a complete calculation for these bands, with an intensity cut-off of 2×10^{-26} cm molecule^{-1}, and the partition function Z equal to 3473 at 296 K. The seven integrated intensities are given in column 4 of Table 5, where the J_{max} and $K_{a\ max}$ reported in columns 2 and 3 are the maximum values of rotational quantum numbers corresponding to the calculation in each of the bands listed in column 1.

3.3.5. Hot bands of $^{16}O_3$: spectral range 1615–2540 cm^{-1}

Twenty hot bands in the 1615–2540 cm^{-1} region, corresponding to transitions from the lower, (0 1 0), (0 0 1) and (1 0 0), states to the upper, (0 1 2), (1 1 1), (2 1 0), (0 0 3), (1 0 2), (2 0 1), (1 3 0) and (3 0 0), states have been included using the known parameters for upper [51] and lower states [51,52] and known transition moment parameters [53–55]. They also appear in the *S&MPO* database. The band intensities and spectral regions of these bands are given in Table 6. The assignment of the bands, the corresponding spectral region, and the band intensity are listed in columns 1–3, respectively.

Table 5
Intensities of the seven ozone strongest bands in the spectral range 2600–3400 cm^{-1}

Band	J_{max}	$K_{a\ max}$	Band intensity (cm molecule^{-1} at 296 K)
$v_2 + 2v_3$	72	19	3.29×10^{-21}
$v_1 + v_2 + v_3$	67	23	2.51×10^{-20}
$2v_1 + v_2$	68	21	8.12×10^{-22}
$3v_3$	70	23	1.41×10^{-19}
$v_1 + 2v_3$	69	21	1.28×10^{-20}
$2v_1 + v_3$	63	23	7.91×10^{-21}
$3v_1$	60	16	4.72×10^{-22}

Table 6
Intensities of ozone hot bands corresponding to (0 1 2), (1 1 1) (2 1 0), (0 0 3), (1 0 2), (2 0 1), (1 3 0), (3 0 0) upper states and (0 1 0), (0 0 1), (1 0 0) lower states

Band	Spectral region (cm^{-1})	Band intensity ($\times 10^{-21}$) ($cm\ molecule^{-1}$ at 296 K)
$v_1+v_2+v_3-v_1$	1617–1706	0.266
$v_2+2v_3-v_3$	1619–1824	0.641
$v_1+v_2+v_3-v_3$	1629–1846	0.125
$v_2+2v_3-v_1$	1642–1706	0.003
$2v_1+v_2-v_1$	1707–1952	0.192
$2v_1+v_2-v_3$	1796–2063	0.011
$3v_3-v_1$	1851–2094	1.177
$v_1+2v_3-v_1$	1871–2069	0.408
$3v_3-v_3$	1876–2096	1.306
$v_2+2v_3-v_2$	1882–2118	3.078
$2v_1+v_3-v_1$	1889–2186	10.992
$v_1+2v_3-v_3$	1933–2082	15.794
$v_1+v_2+v_3-v_2$	1994–2110	43.057
$2v_1+v_3-v_3$	2005–2290	0.306
$3v_1-v_1$	2021–2287	0.467
$2v_1+v_2-v_2$	2051–2282	0.830
$3v_1-v_3$	2077–2310	0.915
$3v_3-v_2$	2258–2360	1.196
$v_1+2v_3-v_2$	2273–2400	0.037
$v_1+3v_2-v_2$	2444–2537	0.013

3.4. N_2O (molecule 4)

The main contribution to the previous content of *GEISA/IASI* related to $^{14}N_2^{16}O$ was by Toth [56–58]. All of the available data reported by Toth data were processed using "the method of effective operator" that was previously applied to CO_2 for the fitting of line positions and line intensities. While the fitting of the line position data of Toth's was found to be satisfactory, some disagreement between calculated and measured band intensities was noted by Lyulin et al. [59]. It is concerned mainly regarding the intensities of the two laser bands, (0001–1000) and (0001–0200), which are centered at 939 and 1056 cm^{-1}, respectively. On the other hand, a comparison of Toth's data with the entries in both the *HITRAN* and *GEISA* databases exhibits a disagreement only in the case of the (0220–0000) forbidden band.

In order to resolve these issues, new and accurate measurements of line intensities were performed using *FTS* facilities at *GSMA* and *LPMA*, and an effective dipole moment was derived using all of the available experimental data on the line intensities in the 10 μm region [60]. While the agreement with Toth's data of the newly measured and calculated line intensities was found to be good, especially in the (0220–0000) band, discrepancies were found to persist still in the (0001–1000) band.

From the above analysis, it turned out that the line intensities in the (0001–1000) and (0220–0000) bands of $^{14}N_2^{16}O$ appearing in *GEISA/IASI* had to be corrected. They have been replaced with the corresponding calculated values obtained from Ref. [60].

Finally, the data on the intensities of 279 lines in the spectral region 870–1240 cm^{-1} were revised in the two bands, $v_3 - v_1$ and $v_3 - 2v_2$, of $^{14}N_2^{16}O$, as the intensities of these lines that were listed before were dubious. In addition, we have removed 118 duplicated lines in the spectral interval 564–629 cm^{-1}.

3.5. CH_4 and CH_3D (molecule 6)

The global database from 0.01 to 6184.5 cm^{-1} on CH_4 and its isotopologue, CH_3D, has been revised in 2001, and the full details about this revision are given by Brown et al. [61]. An extraction of the set of data in the 599–3001 cm^{-1} region from this global database has been included in *GEISA/IASI-03*. Line intensities of the three isotopologues have been scaled according to their natural abundances: 0.988 of $^{12}CH_4$, 0.0111 of $^{13}CH_4$ and 0.000616 of $^{12}CH_3D$.

In the 900–2000 cm^{-1} region, the line positions and line intensities in the two lowest-lying fundamental bands, v_4 at 1310 cm^{-1} and v_2 at 1533 cm^{-1}, were replaced by data obtained using new calculations that were based on the successful modelling of high-resolution laboratory data on $^{12}CH_4$ and $^{13}CH_4$ reported by Champion et al. [62], Brown et al. [63] and Ouardi et al. [64]. Predictions of intensities and some empirical positions [64] were also included. The parameters in three CH_3D fundamentals, v_6 around 1161 cm^{-1}, v_3 around 1307 cm^{-1} and v_5 around 1472 cm^{-1}, were also replaced with data based on new and better calculations by Nikitin et al. [65–68] and Brown et al. [69]. The line parameters, previously appearing in the database, in the bands, v_1, v_3, $2v_4$, $2v_2$, and $v_2 + v_4$, of $^{12}CH_4$ and $^{13}CH_4$ located in the spectral region between 2000 and 3001 cm^{-1}, and in the three fundamentals v_2, v_1, and v_4, in the three combination bands,$v_3 + v_6$, $v_3 + v_5$, and $v_5 + v_6$, and in the three overtone bands, $2v_6$, $2v_3$, and $2v_5$, of $^{12}CH_3D$ were also replaced with new calculations that were based on successful models [70–73] of new measurements. In the case of the hot bands of $^{12}CH_4$, results from Ref. [74] were also included.

The rovibrational transitions of CH_4 are identified using J, C, α, where J is the rotational quantum number, C the symmetry species and α is an index identifying, in increasing order, the levels of increasing energy within the levels with the same value of C. The format in the database had to be altered in order to accommodate the increased range of α from two to three digits.

Experimental data on air-broadened half-widths, (air-) pressure-induced frequency shifts and self-broadened half-widths were inserted for up to 4% transitions of CH_4 and CH_3D [61]. The accuracy in the measured widths is estimated to be 95–98% or better. When experimental data were unavailable, the values of the half-widths estimated in Refs. [67,71] for the lines of $^{12}CH_4$ and $^{13}CH_4$ were employed for most of the transitions. The uncertainties in the estimated values from Refs. [67,71] are about 20%. The value 0.75 adapted for n, the exponent used to describe the temperature dependence of the air-broadened widths of all of the lines previously, was replaced by averaged empirical values from Refs. [76,77] for each value of m, where m is J in the P and Q branches and upper state $J + 1$ in the R branch. While the values of n now exhibit a slight variation with m, the accuracies of these estimates are, perhaps, not better than 55–75%. The following purely empirical expressions were derived as functions of the line position v_i in order to gauge the variation of the (air-) pressure-induced shift with vibrational quanta:

$$\delta^0_{\text{air}} = -0.002 v_i/1300 \quad \text{for } 900-2000\,\text{cm}^{-1}$$

and

$$\delta^0_{\text{air}} = -0.006 v_i/3000 \quad \text{for } 2000-3001\,\text{cm}^{-1}.$$

It should be recognized that the values of the line shift computed using these strictly empirical expressions, which have no proven foundation, could be erroneous by as much as a factor of two for some transitions.

In the case of lines for which experimental data were unavailable, the values of the air-broadened and self-broadened half-widths of the lines of CH_3D derived using the empirical expressions presented in Ref. [61] were introduced into the database. For most transitions, the expressions used were:

$$\gamma_{\text{air}} = 0.0677 - 5.681 \times 10^{-5} m - 8.397 \times 10^{-5} k^2,$$

$$\gamma_{\text{self}} = 0.0869 - 6.41 \times 10^{-5} m - 6.56 \times 10^{-5} k^2,$$

where m is as described above. k is the quantum number K in the lower energy level for transitions with $\Delta K = -1$ and 0, and the K of the upper level for transitions with $\Delta K = +1$. Different expressions were required for transitions with $J'' = K''$, the ^{P}P, ^{Q}Q, ^{R}R lines. They are

$$\gamma_{\text{air}} = 0.06863 - 3.762 \times 10^{-4} m + 7.044 \times 10^{-7} m^2$$

and

$$\gamma_{\text{self}} = 0.0875 - 3.46 \times 10^{-4} m + 4.94 \times 10^{-7} m^2.$$

Although the measured data on the air-broadened and self-broadened half-widths of the lines of CH_3D were reported to have an uncertainty that does not exceed 3%, those data could be reproduced by the empirical expressions within an uncertainty of 6–7% only. In the case of all of the unmeasured transitions of CH_3D, δ^0_{air} has taken to be equal to $-0.0025 v_i/1300$, and the temperature dependence of the air-broadened widths was set to be determined by a constant value, 0.75, of the exponent n.

Further improvements are not contemplated to be introduced into the next update of this database for the lines of methane in the 900–3000 cm^{-1} spectral region, but a number of new measurements and theoretical studies are definitely needed. The needs that are apparent are as follows. We need a better characterization of the "hot" bands in the 3.3 μm region, a more thorough measurement of the air-broadened and self-broadened half-widths of weaker transitions around 8 μm, including values of n, line-mixing studies in the fundamental bands, and, most importantly, theoretical models that can reproduce the existing measured half-widths of the lines of $^{12}CH_4$ and $^{12}CH_3D$ with better accuracy.

3.6. NO (molecule 8)

The air-broadened half-widths and the (air-) pressure-induced shifts of lines in the 1487–2188 cm^{-1} spectral region have been updated using the data from [78–80].

3.7. NO_2 (molecule 10)

In 1999, a new line list was set up in the spectral region of the $\nu_1+\nu_3$, $\nu_1+2\nu_2$, and $\nu_1+\nu_2+\nu_3-\nu_2$ bands of $^{14}N^{16}O_2$. Line positions and intensities are from Ref. [81]. Air-broadened half-widths were calculated by using an empirical polynomial of the rotational quantum number N of the lower energy level of the transition. It was derived by fitting it to a wide-ranging set of data on nitrogen-broadened and oxygen-broadened half-widths measured by Dana et al. [82]. The same expansion was used for the three bands under the assumption that there is no dependence on vibrational quantum numbers. The exponent n in the expression for the temperature dependence of the air-broadened half-widths was taken from experimental studies [83–85]. Refs. [83,84] deal with nitrogen-broadened half-widths of lines in the ν_3 band, while Ref. [85] deals with air-broadened half-widths of a few lines in the ν_3 band. A mean value $n=1$ was then fixed for all lines for the lack of a well-defined value for each of the lines. As data on (air-) pressure-induced line shifts were unavailable, a zero was assigned to that parameter in all of the entries. Self-broadened half-widths of all of the lines have been fixed to be the average value of $0.095\,cm^{-1}\,atm^{-1}$ at 296 K, which was derived from the experimental results of Perrin et al. [86]. This means, of course, that any dependence of this parameter on vibrational quantum numbers has been ignored.

3.8. C_2H_2 (molecule 24)

The update of the spectral line parameters of acetylene is in the 5-, 7.5- and 13.7-μm spectral regions. It is derived from Refs. [87–91].

The levels are designated as $(v_1,v_2,v_3,v_4,v_5,\ell\pm r$, with $\ell=|\ell_4+\ell_5|)$, where v_t and ℓ_t are the usual vibrational quantum numbers, $\pm$ being the symmetry type for Σ vibrational states, and r a roman numeral (or the corresponding digit in the files), indicating the rank of the level, by decreasing energy value ($r=I$ for the highest energy level), inside the set of states having the same vibrational symmetry, and coupled by ℓ-type resonances. When the two last indications are unnecessary, they are replaced by underscores ("_"). These notations are illustrated in Table 7. In the first column, the usual comprehensive notation of the vibrational levels is given. The second column contains a more rigorous full spectroscopic notation of these levels. The third column gives the code adopted in *GEISA/IASI-03*.

We have revised the database on the lines in the 13.6 μm region using the latest measurement of the line intensities [87,88]. The main improvement is in the line intensities and transition dipole moment of $^{12}C_2H_2$. The data on $^{12}C^{13}CH_2$ have not been revised.

In the 7.5 μm (1248–1415 cm^1) region, the data are on the lines of the $(\nu_4+\nu_5)^0_+$ combination band. Line positions, intensities (including the square of the transition dipole moment), and lower level energies have been updated by drawing upon Ref. [91]. The notable difference between the revised and the previous line intensities is recognition of significant Herman–Wallis factors, which were interpreted to be due to l-type resonance and Coriolis coupling affecting the upper level of the transition. The calculated line intensities included in the database are also from Ref. [91]. The improvement achieved in including the Herman–Wallis factors ranges from +4.5% for the P(17) line to −19% for the R(35) line. The accuracy of the line intensities was estimated to be 2% in Ref. [91]. Line positions and lower level energies were calculated using the model of Kabbadj et al. [92] and the constants listed in Table 3 of that work. The uncertainty in the wavenumbers of the transitions is slightly better than $10^{-4}\,cm^{-1}$. The other parameters have not been changed.

Table 7
List of C_2H_2 vibrational levels

Level	Notation	Code
Ground state	000000 + _	1
v_5^1	000011__	2
v_3	001000 + _	3
$v_2 + (v_4 + v_5)^0_+$	010110 + _	4
v_4^1	000101__	5
$(v_4 + v_5)^0_-$	000110−_	6
$(v_4 + v_5)^0_+$	000110 + _	7
$(v_4 + v_5)^2$	000112__	8
$2v_5^0$	000020 + _	9
$2v_5^2$	000022__	10
$3v_5^1$	000031__	11
$(2v_4 + v_5)^1$II	000211_2	12
$(2v_4 + v_5)^1$I	000211_1	13
$(3v_4 + v_5)^0_+$	000310 + _	14
$(3v_4 + v_5)^0_-$	000310−_	15
$(3v_4 + v_5)^2$II	000312_2	16
$(3v_4 + v_5)^2$I	000312_1	17
$v_2 + v_5^1$	010011__	18
$(v_4 + 3v_5)^0_+$	000130 + _	19
$(v_4 + 3v_5)^0_-$	000130−_	20
$(v_4 + 3v_5)^2$II	000132_2	21
$(v_4 + 3v_5)^2$I	000132_1	22
$v_2 + v_4^1$	010101__	23
$(2v_4 + 2v_5)^0_+$ II	000220 + 2	24
$(2v_4 + 2v_5)^0_-$	000220−_	25
$(2v_4 + 2v_5)^2$II	000222_2	26
$4v_5^0$	000040 + _	27
$4v_5^2$	000042__	28

A line list has been introduced on the lines of $^{12}C_2H_2$ in the 5 μm region. The source of these data is Refs. [89,90]. Air-broadened half-widths are from [93–95,97]. The paper by Babay et al. [96] is the source for the air-induced line shifts. Ref. [97] is the source for the information on the temperature dependence of the air-broadened half-widths.

4. Summary of the updates for individual line parameters in GEISA/IASI-03

A general summary of the updates per molecule, as presented in Section 3, is given in Table 8.

Fig. 1 details the line coverage and the evolution of *GEISA/IASI* content since 1997, for each of the eight updated molecular species as shown in panels (a) to (i) (two panels for H_2O). On the left

Table 8
Summary of new data in *GEISA/IASI-03* sub-database on line transition parameters

Molecule	# lines	Intensity average (cm molecule^{-1})	Alpha[a] average (cm^{-1} atm^{-1})	Isotope	# lines	Minimum wavenumber (cm^{-1})	Maximum wavenumber (cm^{-1})	Minimum intensity (cm molecule^{-1})	Maximum intensity (cm molecule^{-1})
H_2O (Toth)	10,363	1.04×10^{-21}	0.065	161	4,776	599.681	2819.848	2.02×10^{-27}	2.99×10^{-19}
				181	1,599	604.933	2310.511	2.02×10^{-27}	6.05×10^{-22}
				171	1,119	599.702	2260.604	2.02×10^{-27}	1.21×10^{-22}
				162	2,256	604.366	1921.278	2.02×10^{-27}	2.51×10^{-23}
				182	438	1173.772	1684.226	2.02×10^{-27}	5.08×10^{-26}
				172	175	1234.235	1598.765	2.02×10^{-27}	9.32×10^{-27}
H_2O (RAL)	2232	7.90×10^{-24}	0.057	161	1,075	700.032	1299.735	1.00×10^{-27}	1.91×10^{-21}
				181	235	701.653	1298.160	2.03×10^{-27}	3.84×10^{-24}
				171	132	702.262	1294.719	2.05×10^{-27}	7.18×10^{-25}
				162	694	700.558	1299.980	2.02×10^{-27}	1.38×10^{-23}
				182	81	1173.772	1299.865	2.06×10^{-27}	2.78×10^{-26}
				172	15	1234.235	1293.770	2.06×10^{-27}	5.12×10^{-27}
CO_2	44,748	2.46×10^{-21}	0.071	627	7,579	599.183	2806.199	1.00×10^{-27}	1.25×10^{-21}
				626	18,038	599.222	2488.222	1.00×10^{-27}	3.53×10^{-18}
				636	7,265	599.026	2395.279	1.00×10^{-27}	3.75×10^{-20}
				628	11,866	599.007	2826.650	1.00×10^{-27}	6.84×10^{-21}
O_3	142,591	1.10×10^{-22}	0.069	666	109,307	600.179	3000.971	2.98×10^{-26}	4.06×10^{-20}
				668	13,728	640.037	1177.493	9.68×10^{-26}	7.76×10^{-23}
				686	19,556	640.141	2259.896	9.97×10^{-29}	7.56×10^{-23}
N_2O	279	1.05×10^{-23}	0.073	446	279	872.399	1243.755	1.28×10^{-28}	3.73×10^{-23}
CH_4	121,281	6.89×10^{-23}	0.050	211	68,777	922.651	3000.998	1.00×10^{-27}	1.20×10^{-19}
				311	22,688	998.884	3000.999	9.49×10^{-28}	1.34×10^{-21}
				212	29,816	855.753	3000.997	6.16×10^{-29}	3.66×10^{-23}
NO	9610	4.78×10^{-22}	0.050	46	9,610	1,487.366	2188.447	1.110×10^{-39}	2.32×10^{-20}
NO_2	9110	3.23×10^{-22}	0.069	646	9,110	2719.056	2992.323	9.92×10^{-26}	6.64×10^{-21}
C_2H_2	2904	1.11×10^{-20}	0.070	221	2,754	604.774	2254.963	9.49×10^{-27}	1.19×10^{-18}
				231	150	613.536	843.872	3.82×10^{-26}	1.58×10^{-20}

[a] Lorentzian air collision half-width at 296 K.
Column 1: Molecular species archived in *GEISA/IASI-03*.
For each molecular species listed in column 1:
Column 2: Total number of lines.
Column 3: Intensity average (cm molecule^{-1} at 296 K).
Column 4: Mean half-width at half maximum (cm^{-1}).
Column 5: Isotope identification codes [4].

For each isotope listed in column 5:
Column 6: Number of lines.
Column 7: Transition minimum wavenumber (cm^{-1}).
Column 8: Transition maximum wavenumber (cm^{-1}).
Column 9: Lines minimum intensity (cm molecule^{-1} at 296 K).
Column 10: Lines maximum intensity (cm molecule^{-1} at 296 K).

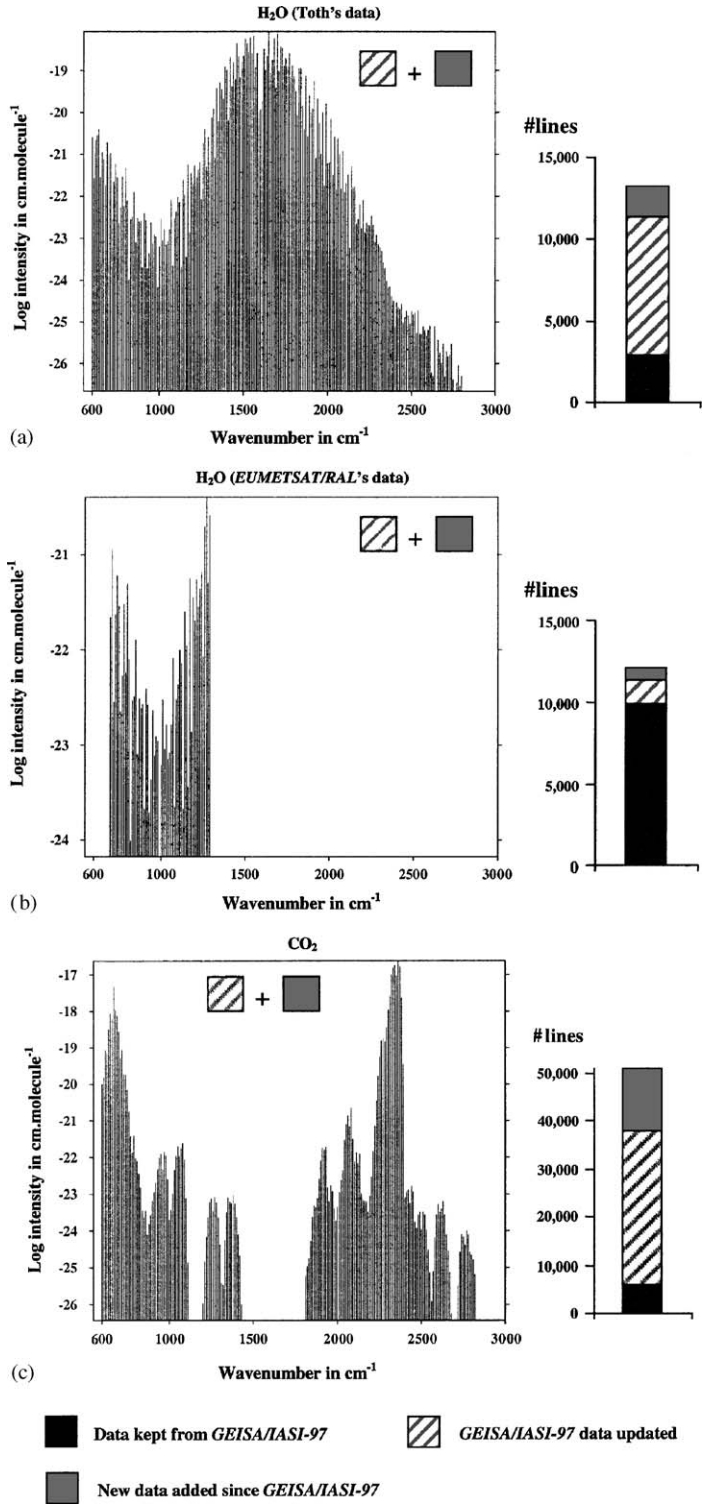

Fig. 1. Updates and additions in *GEISA/IASI-03* individual line parameters sub-database. Evolution of the database content since 1997.

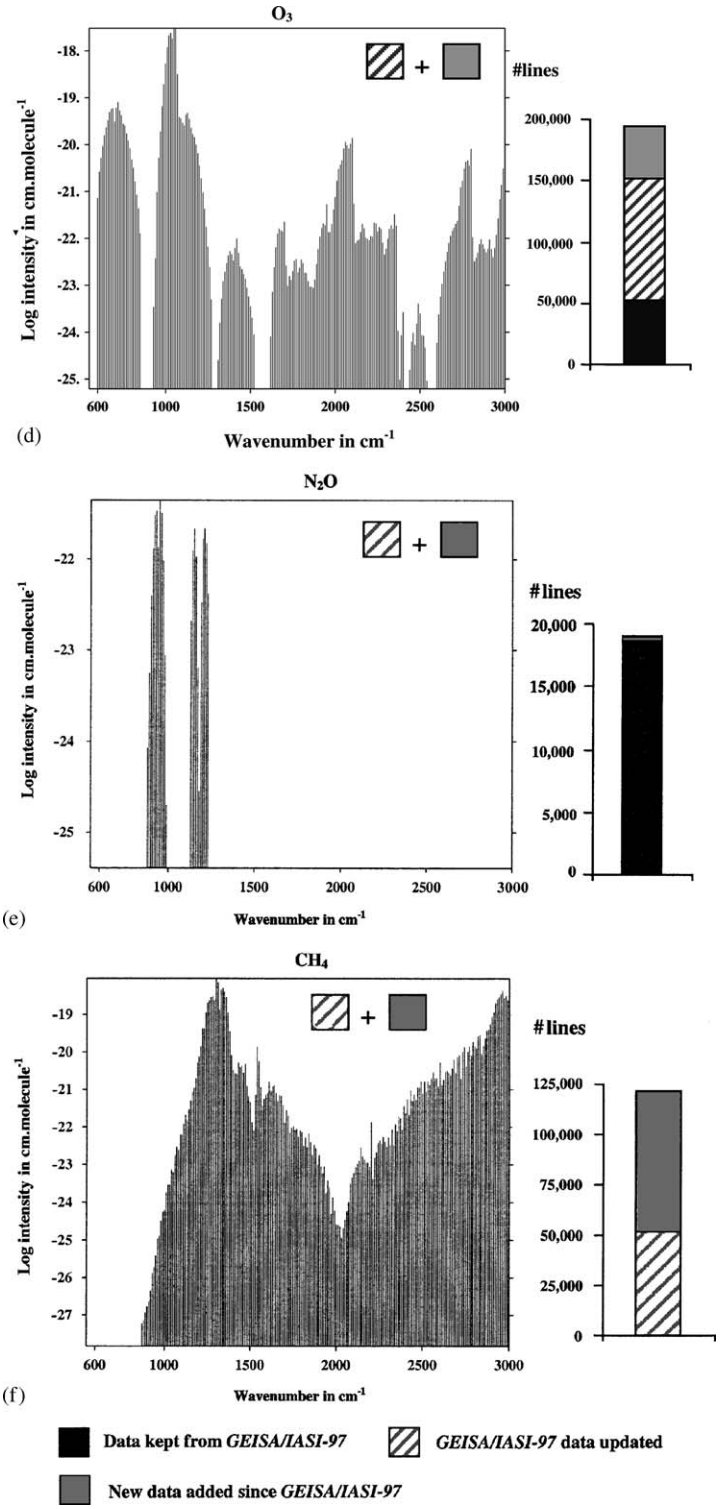

Fig. 1. (*Continued*)

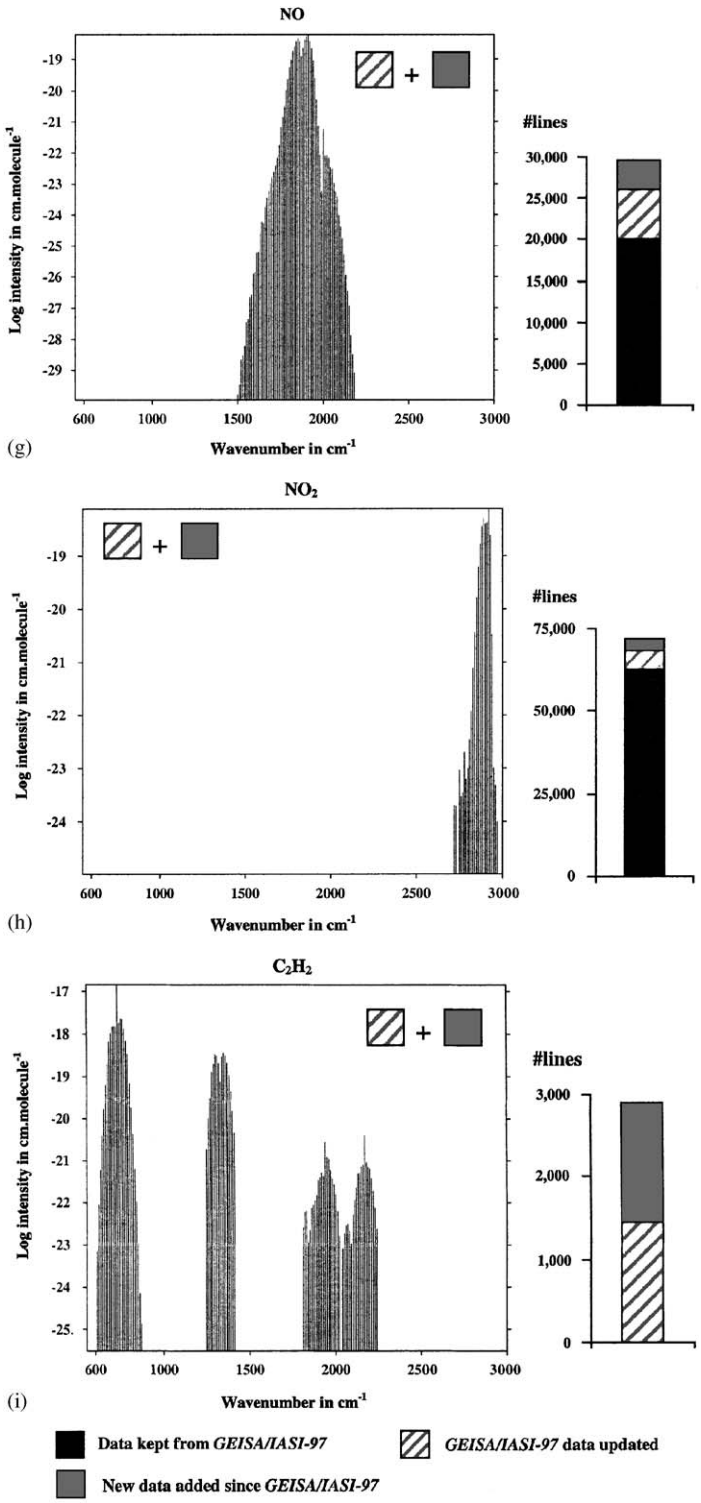

Fig. 1. (*Continued*)

side of a panel, the logarithm of the intensities of the updated or added lines, averaged over 10 cm^{-1} intervals, are plotted versus the GEISA/IASI spectral range (from 599 to 3001 cm^{-1}). The associated histogram, on the right side of a panel, gives the total number of lines and illustrates the evolution of the individual line content in the database since 1997. The lines have been sorted into three categories, i.e.: kept identical, updated, added, in *GEISA/IASI-03*.

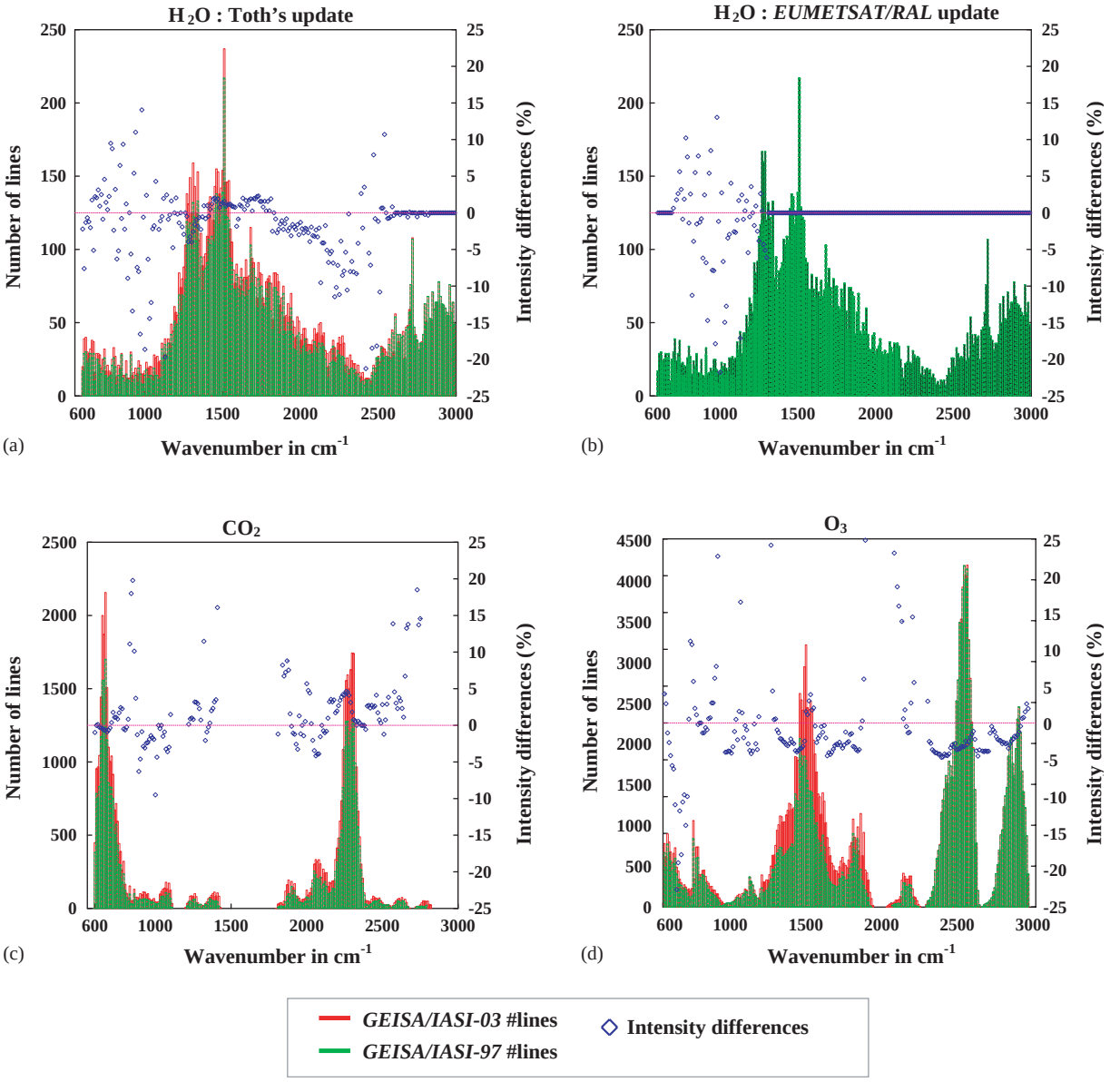

Fig. 2. Update impacts in *GEISA/IASI-03* individual line parameters sub-database: line content (left-hand Y-axis) and line intensities (right- hand Y-axis).

Illustrations of the impact of the updates of *GEISA/IASI-97*, through 2001–2003, in terms of database total line content per molecule and differences in % line intensities, are presented in the series of plots of Fig. 2. These plots, labelled from (a) to (d), are related respectively to: H_2O (Toth's update in panel (a) and *EUMETSAT/RAL* update in panel (b)), CO_2 (panel (c)) and O_3 (panel (d)). The same $10\,cm^{-1}$ average as in Fig. 1 has been applied to the values of the line numbers (left) and of the percent intensities (right-hand Y-axis), expanded from 599 to $3001\,cm^{-1}$ on the X-axis. The spectral lines intensity differences, in percent, have been evaluated with the formula:

$$(I_{03} - I_{97})/I_{97} \times 100.$$

I_{03} and I_{97} identify the spectral lines intensity values in *GEISA/IASI-03* and in *GEISA/IASI-97,* respectively.

Default values have been chosen for missing data values, i.e.: $-1.0\,cm^{-1}$ for the energy of the lower transition level and $-0.9999\,cm^{-1}\,atm^{-1}$ at 296 K for the Lorentzian collision half-width.

5. The GEISA/IASI-03 sub-database on infrared absorption cross-sections

For the analysis of atmospheric spectra to be recorded by the *IASI* instrument, broadband absorption features associated with infrared absorption of heavy molecules, such as CFCs and substitutes, have to be taken into account.

For these heavy molecules, the spectral lines cannot be resolved by the measurements and hence their spectroscopy has to be characterized in terms of absorption cross-sections. Compiling reference absorption cross-sections corresponding to a wide range of pressure and temperature conditions is essential for performing accurate radiative transfer calculations.

The *GEISA/IASI-03* absorption cross-sections sub-database contains 6,572,329 entries related to six molecules, i.e.: CFC-11, CFC-12, CFC-14, HCFC-22, N_2O_5 and CCl_4 (newly archived).

As in the previous editions of the database [4,7], the archived absorption cross-sections are determined through the following expression:

$$\sigma(\omega) = \frac{\ln[I_0(\omega)/I(\omega)]}{nl},$$

where ω is the wavenumber (cm^{-1}), $\sigma(\omega)$ the absorption cross-section ($cm^2 molecule^{-1}$), $I_0(\omega)$ and $I(\omega)$ the intensities at the wavenumber ω, of the incident and transmitted radiation, respectively, n the concentration of the absorbing molecules ($molecule\,cm^{-3}$), l the optical path length (cm).

A data management program is associated with this sub-database.

Table 9, split into three parts, details the fields of the format in the data archive. Part (a) gives the fields of the format for the absorption cross-sections data file itself. The related molecule identification codes are provided in part (b). Each cross-section value is associated with one of 274 listed atmospheric conditions and coded as summarized in part (c), following their specific temperature, pressure and spectral resolution.

Recent efforts have supplemented the previous edition [7] of the *GEISA/IASI* absorption cross-sections sub-database. This has represented an increase of 275% in data amount in the archive, the content of which is summarized in Table 10. For each molecular species listed in column 1,

Table 9
Fields of the format for data archive in *GEISA/IASI-03* absorption cross-sections sub-database

(a) *Absorption cross-section parameters data format*

Parameter	Wavenumber (cm^{-1})	Absorption cross-section (cm^2 $molecule^{-1}$)	Molecule identification code	Atmospheric condition code
Fortran descriptor	F12.6	1PE10.3	I3	I3

(b) *Molecule identification codes*

Molecule	CFC-11	CFC-12	CFC-14	HCFC-22	N_2O_5	CCl_4
Identification code	1	2	4	16	23	26

(c) *Atmospheric condition codes file data format:*

Parameter	Atmospheric conditions code	Temperature (K)	Pressure (Pa)	Resolution (cm^{-1})	Internal *GEISA* code for data identification
Fortran descriptor	I3	F9.1	F12.2	F7.3	A1

Part (a):
Column 1: Wavenumber (cm^{-1}).
Column 2: Absorption cross-section (cm^{-2} $molecule^{-1}$).
Column 3: Molecule identification code.
Column 4: Atmospheric condition code.

Part (c):
Column 1: Atmospheric condition code.
Column 2: Temperature (K).
Column 3: Pressure (Pa).
Column 4: Resolution (cm^{-1}).
Column 5: Internal *GEISA* code for data identification.

and per related reference listed in column 6, are given, in columns 2–4: the ranges for, the spectral interval (cm^{-1}), the temperature (K) and the pressure (Pa); the numbers of T, P (Temperature, Pressure) sets and of entries are in columns 5 and 7, respectively. A zero value of the pressure corresponds to pure vapour data. In the last line of the table are displayed, for the sub-database as a whole, the total numbers of T, P sets (column 5) and of entries (column 7).

Fig. 3, split in panels (a)–(f), details the T, P and the database evolution since 1997, for the six archived molecular species. Per molecule, identified on the left side of a panel divided into two sections: the above section is related with pure vapour cross-sections (either corresponding to a pure gas-non-air-broadened or extrapolated to zero pressure from a set of laboratory data); on the below section, related with air-broadened gas, the displayed T (in K, on the X axis), P (in hPa, on the Y-axis) sets are associated with five *TIGR*-2000 [116,117] atmospheric temperature and

Table 10
Summary of *GEISA/IASI-03* absorption cross-sections sub-database content

Molecule	Spectral range (cm^{-1})	Temperature range (K)	Pressure range (Pa)	# T,P sets	References	# entries
CFC-11	599–2000	296	93,325	1	Hurley [98]; Christidis [99]	
(CCl_3F)	500–1601	297	0	1	Heathfield [100]; Smith [101]	1,657,853
	810–880 1050–1120	190–296	1000–101,325	55	Li and Varanasi [102]; Varanasi [103]	
CFC-12	850–1190	253–287	0	3	Clerbaux [104]	
(CCl_2F_2)	210–2000	296	93,325	1	Hurley [98]	2,199,538
	850–950	190–296	1000–101,392	57	Varanasi and Nemtchinov [105]; Varanasi [103]	
	1050–1120					
CFC-14	220–2000	296	93,325	1	Hurley [98]	411,228
(CF_4)	1250–1290	180–296	1005–101,458	55	Nemtchinov and Varanasi [106]	
HCFC-22	700–1500	203–293	0–80,000	8	Vander Auwera [107] Ballard et al. [108]	
($CHClF_2$)	765–1380	253–287	0	3	Clerbaux [104]	2,019,054
	208–2000	296	93,325	1	Pinnock [109]; Hurley [98]	
	760–860 1070–1195	181–297	2666–101,936	51	Varanasi [110,111] Varanasi et al. [112]	
N_2O_5	540–1380	205–293	0	5	Wagner and Birk [113,114]	87,120
CCl_4	750–812	208–297	1070–101,272	32	Nemtchinov and Varanasi [115]	197,536
Total				274		6,572,329

pressure profiles. The associated histogram, on the right part of the panel, gives the total number of cross-sections, in *GEISA/IASI-97* (left plot) and in *GEISA/IASI-03* (right plot), as an illustration of the evolution of the database.

6. The GEISA/IASI-03 sub-database on microphysical and optical properties of atmospheric aerosols

Besides the molecular species which define the gaseous infrared opacity in the Earth's atmosphere, aerosol particles, however, also contribute to this opacity. Consequently, a common

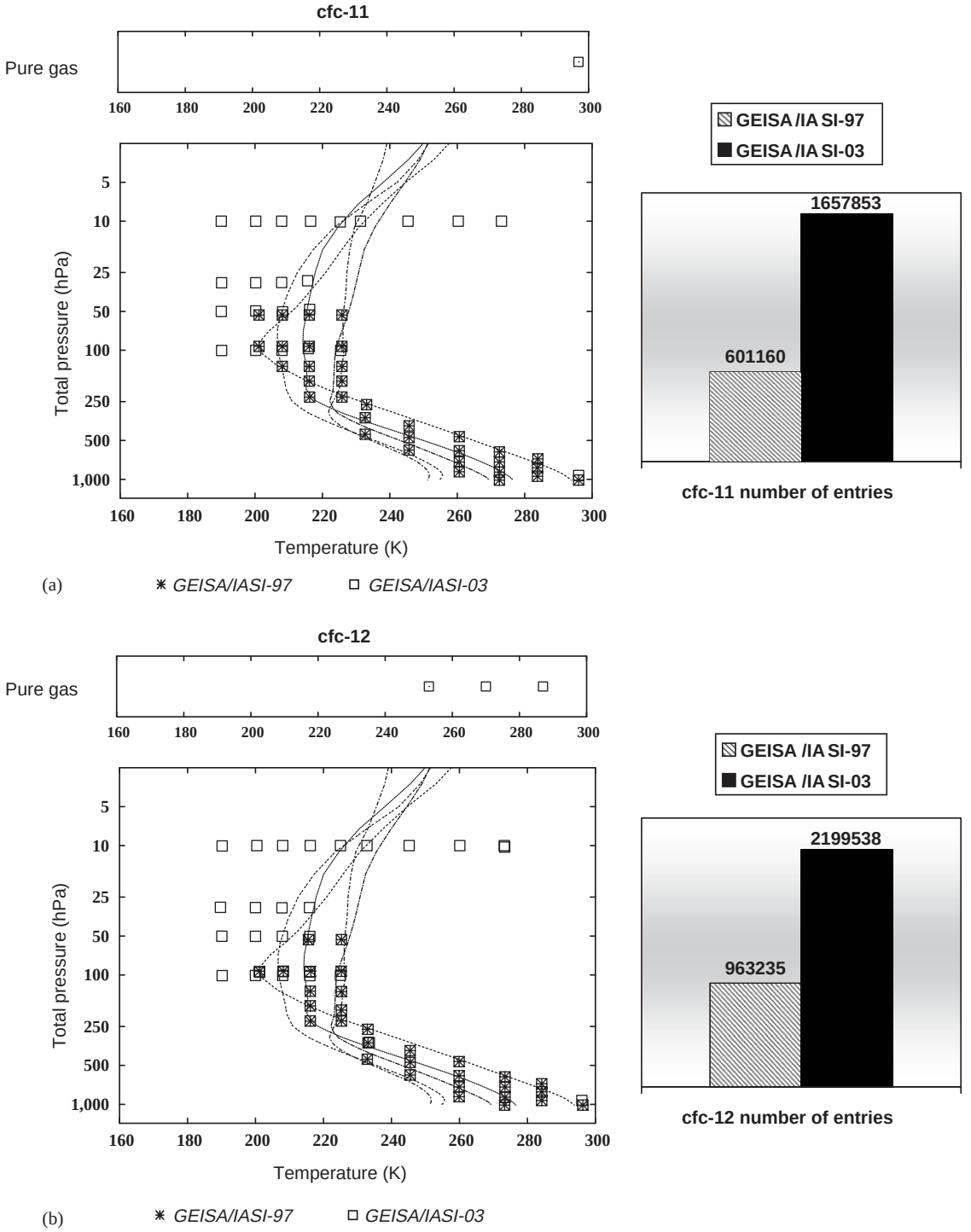

Fig. 3. *GEISA/IASI-03* cross-sections sub-database. *T*, *P* distribution and evolution since *GEISA/IASI-97*. On each panel: 5 *TIGR-2000* [116,117] atmospheric *T*, *P* profiles, i.e.: 5 = polar1, 4 = polar2, 3 = mid-latitude2, 2 = mid-latitude1, 1 = tropical atmospheres (see panel (f) for identification).

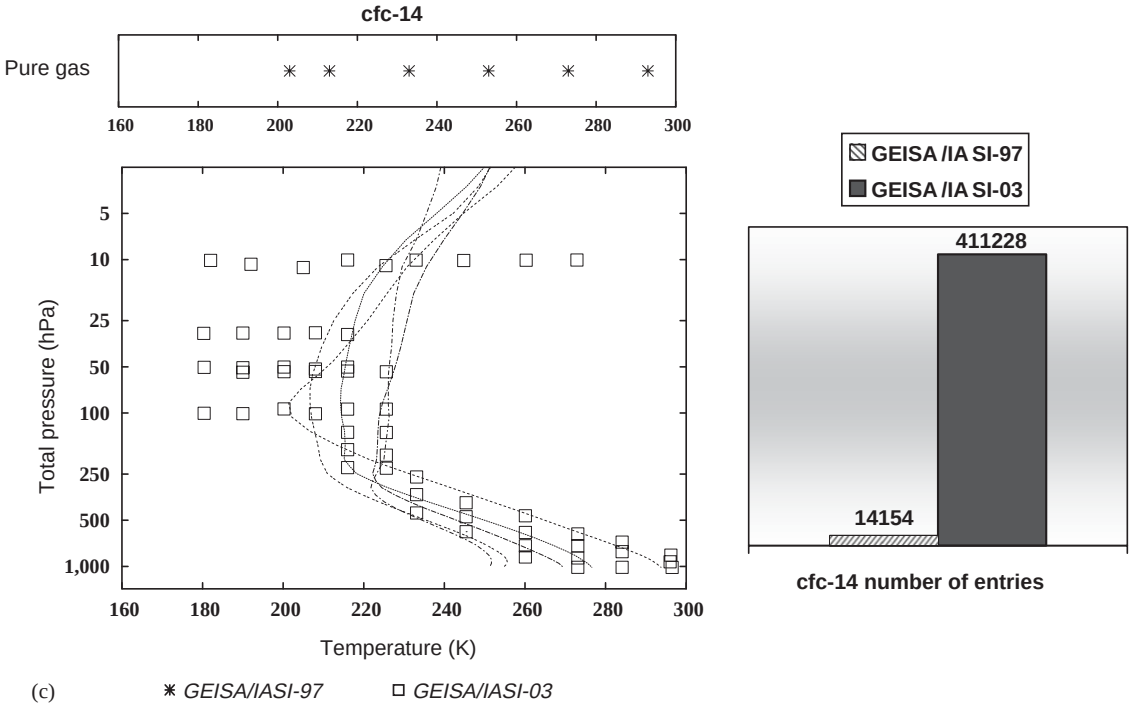

(c) ✳ *GEISA/IASI-97* □ *GEISA/IASI-03*

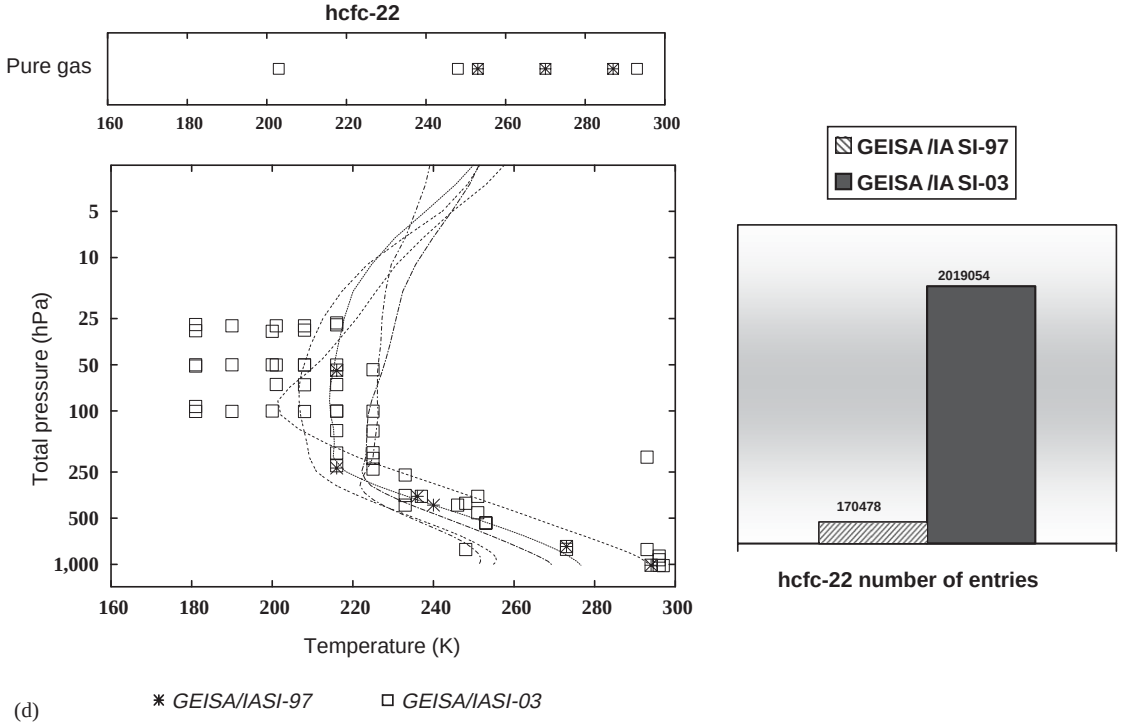

(d) ✳ *GEISA/IASI-97* □ *GEISA/IASI-03*

Fig. 3. (*Continued*)

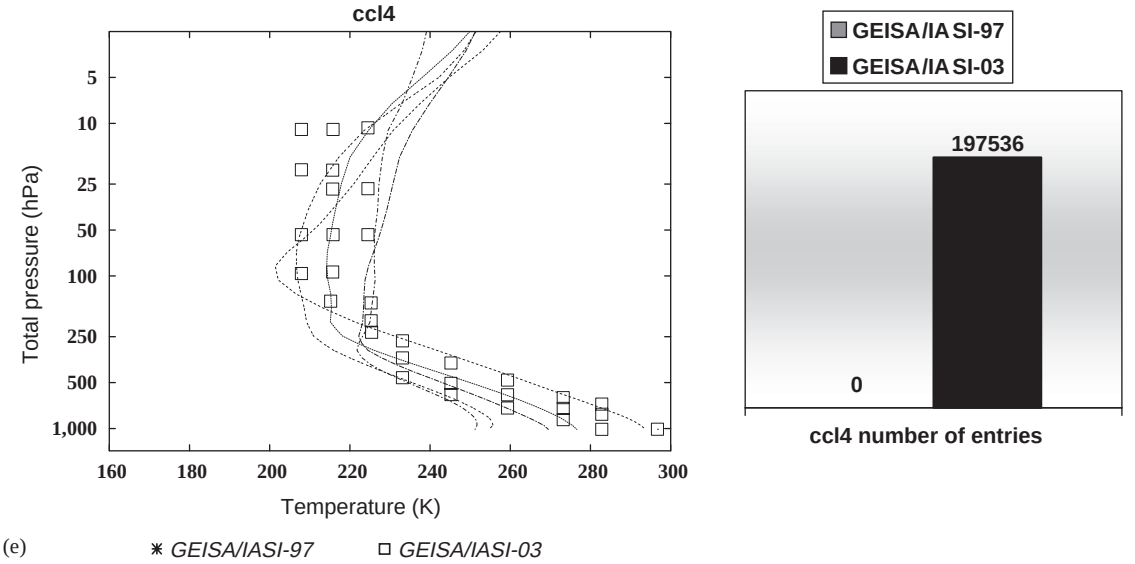

(e)

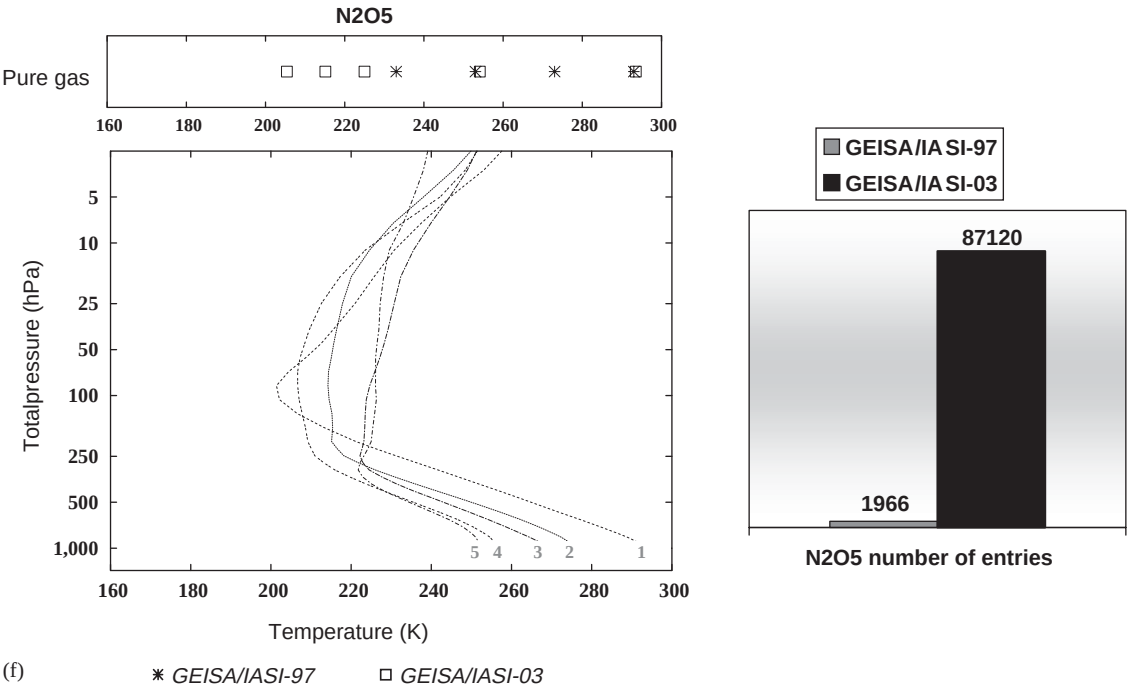

(f)

Fig. 3. (*Continued*)

GEISA and *GEISA/IASI* aerosol sub-database has been elaborated. It gathers the micro-physical and optical properties and possibly computed optical related properties, for selected basic aerosol components, from four published aerosol data catalogs, i.e.:

- A database on refractive indices of 10 varieties of basic aerosol components [118–120].
- A database on basic aerosol components and service software [121].
- The database and associated software package *OPAC* [122].
- The *GADS* data set [123].

Ternary solution droplets are an important composition type of *P*olar *S*tratospheric *C*louds. Norman et al. [124] recently published real and imaginary ternary indices at 220 K at six different ternary compositions, and these indices will be added to the next *GEISA-IASI* edition.

This aerosols sub-database has been extensively described in Ref. [7], related with the 2001 Edition of *GEISA/IASI*. It is available from the *ARA/LMD* group workstations web site (see next paragraph). No update has occurred since that time.

7. GEISA/IASI management software and availability

Management software and user's friendly facilities are associated with the *GEISA/IASI* system.

- *The individual line parameters sub-database* management software package has been updated and includes new functionality, since the former editions of *GEISA* [4] and *GEISA/IASI* [7]. The user has the choice of:
  - to make data extractions by molecule, isotopomer and quantum identification, between two given wavenumbers;
  - to analyse selected sampled spectral intervals, in terms of line intensities and/or energy of the lower transitions, thanks to the plots of related histograms;
  - to obtain a complete description of the line parameters content for each molecular species, i.e. for each existing transition, the number of lines, the wavenumber interval and the intensity minimum and maximum values are provided.

  Among the new software utilities, one of the most important is the possible conversion of any *GEISA/IASI* format file into the new *GEISA* [8,9] format (the two formats are very close) and/or into the *HITRAN*-2000 one [27]. Newly, the software also allows to transform any spectroscopic data file into one in the *GEISA/IASI* format and to make comparisons between two spectroscopic data files. Finally, it is possible to mix, in an intelligent way, two different files for an accurate update, avoiding duplicated information, especially in the database update process.
- *The cross-sections sub-database* management software allows:
  - to make extraction of data, by temperature, pressure and T, P set;
  - to list the available T, P sets for each molecule;
  - to obtain a detailed description of the information available for each molecular species, i.e.: for each available T, P set, the number of records, the wavenumber interval and the intensity minimum and maximum values are given.

These management software facilities are interfaced on the *ARA/LMD* group web site at: http://ara.lmd.polytechnique.fr. They are also accessible at the *GEISA* restricted free access ftp site:

http://ara.lmd.polytechnique.fr/ftpgeisa. Previously, the potential user required a login and a password, at the *ARA/LMD* web site.

Acknowledgements

This research funded by *CNES* is supported by *EUMETSAT* in the frame of the *EPS/METOP* project. Both institutions are acknowledged for their encouragements.

References

[1] Chédin A, Husson N, Scott NA. Une banque de données pour l'étude des phénomènes de transfert radiatif dans les atmosphères planétaires: la banque GEISA. Bull. Inform. Centre Données Stellaires (France) 1982;22:121–121.

[2] Husson N, Bonnet B, Scott NA, Chédin A. Management and study of spectroscopic information: the GEISA program. JQSRT 1992;48:509–18.

[3] Husson N, Bonnet B, Chédin A, Scott NA, Chursin AA, Golovko VF, Tyuterev VlG. The GEISA data bank in 1993. A PC/AT compatible computers' new version. JQSRT 1994;52:425–38.

[4] Jacquinet-Husson N, Arié E, Ballard J, Barbe A, Bjoraker G, Bonnet B, Brown LR, Camy-Peyret C, Champion J-P, Chédin A, Chursin AA, Clerbaux C, Duxbury G, Flaud J-M, Fourrié N, Fayt A, Graner G, Gamache R, Goldman A, Golovko Vl, Guelachvilli G, Hartmann J-M, Hilico J-C, Hillman J, Lefèvre G, Lellouch E, Mikhailenko SN, Naumenko OV, Nemtchinov V, Newham DA, Nikitin A, Orphal J, Perrin A, Reuter DC, Rinsland CP, Rosenmann L, Rothman LS, Scott NA, Selby J, Sinitsa LN, Sirota JM, Smith AM, Smith KM, Tyuterev VlG, Tipping RH, Urban S, Varanasi P, Weber M. The 1997 spectroscopic GEISA databank. JQSRT 1999;62:205–54.

[5] Jacquinet-Husson N, Scott NA, Chédin A, Bonnet B, Barbe A, Tyuterev VlG, Champion J-P, Winnewisser M, Brown LR, Gamache R, Golovko Vl, Chursin AA. The GEISA system in 1996: toward an operational tool for the second generation vertical sounders radiance simulation. JQSRT 1998;59:511–27.

[6] Jacquinet-Husson N, Scott NA, Chédin A, Barbe A, Tyuterev VlG, Champion J-P, Winnewisser M, Brown LR, Gamache R, Golovko Vl, Chursin AA. The 1997 spectroscopic GEISA database system and the second generation vertical sounders radiance simulation. Proceedings of the Ninth Conference on Satellite Meteorology & Oceanography, Paris, France, 25–29 May 1998. p. 682–85.

[7] Jacquinet-Husson N, Scott NA, Chédin A, Chursin AA. The GEISA spectroscopic database system updated for IASI direct radiative transfer modelling. Atmos Ocean Opt 2003;16:256–61.

[8] Jacquinet-Husson N, Scott NA, Garceran K, Armante R, Chédin A, Lefèvre G, Barbe A, Birk M, Camy-Peyret C, Chance K, Chursin AA, Claveau C, Clerbaux C, Coheur PF, Dana V, Daumont L, Debacker-Barilly MR, Fally S, Flaud J-M, Goldman A, Hamdouni A, Hess M, Hurley MD, Jacquemart D, Kleiner I, Köpke K, Mandin JY, Massie S, Mikhaïlenko SN, Newnham D, Nemtchinov V, Nikitin A, Orphal J, Perrin A, Régalia-Jarlot L, Rublev A, Schreier F, Schult L, Smith KM, Tashkun SA, Teffo J-L, Tyuterev VlG, Vander Auwera J, Varanasi P, Wagner G. The 2003 Edition of GEISA: a spectroscopic database system for the second generation vertical sounders radiance simulation. Proceedings of the 13th international TOVS study conference (ITSC-13), Sainte-Adèle, Canada, 28 October–4 November 2003.

[9] Jacquinet-Husson N, Scott NA, Garceran K, Armante R, Chédin A, Lefèvre G, Barbe A, Birk M, Camy-Peyret C, Chance K, Chursin AA, Claveau C, Clerbaux C, Coheur PF, Dana V, Daumont L, Debacker-Barilly MR, Fally S, Flaud J-M, Goldman A, Hamdouni A, Hess M, Hurley MD, Jacquemart D, Kleiner I, Köpke K, Mandin JY, Massie S, Mikhaïlenko SN, Newnham D, Nemtchinov V, Nikitin A, Orphal J, Perrin A, Régalia-Jarlot L, Rublev A, Schreier F, Schult L, Smith KM, Tashkun SA, Teffo J-L, Tyuterev VlG, Vander Auwera J, Varanasi P, Wagner G. The 2003 edition of the GEISA spectroscopic database. JQSRT 2005 (in preparation).

[10] Scott NA, Chedin A. A fast line-by-line method for atmospheric absorption computations: the automatized atmospheric absorption atlas. J Appl Meteor 1981;20:556–64.
[11] Tournier B, Armante R, Scott NA. STRANSAC-93 et 4A-93: Développement et validation des nouvelles versions des codes de transfert radiatif pour application au projet IASI. Internal Rep. LMD, No. 201, LMD/CNRS, Ecole Polytechnique, PALAISEAU, France; 1995.
[12] Chéruy F, Scott NA, Armante R, Tournier B, Chédin A. Contribution to the development of radiative transfer models for high spectral resolution observations in the infrared. JQSRT 1995;53:597–611.
[13] Toth RA. Private communication; 2000.
[14] Stewart BC, editor. Support study on water vapor spectroscopy for IASI. Final report. EUMETSAT Contract EUM/CO/01/939/DK. 2003. p. 1–159.
[15] Toth RA. The v_2 band of $H_2^{16}O$—line strengths and transition frequencies. J Opt Soc Am B 1991;8:2236–55.
[16] Toth RA. Transition frequencies and absolute strengths of $H_2^{17}O$ and $H_2^{18}O$ in the 6.2 μm region. J Opt Soc Am B 1992;9:462–82.
[17] Toth RA. Water vapor measurements between 590 and 2582 cm^{-1}: line positions and strengths. J Mol Spectrosc 1998;190:379–96.
[18] Toth RA. $HD^{16}O$, $HD^{18}O$, and $HD^{17}O$ transition frequencies and strengths in the v_2 bands. J Mol Spectrosc 1993;162:20–40.
[19] Toth RA. HDO and D_2O low pressure, long path spectra in the 600–3100 cm^{-1} region I. HDO line positions and strengths. J Mol Spectrosc 1999;195:73–97.
[20] Toth RA. Analysis of line positions and strengths of $H_2^{16}O$ ground and hot bands connecting to interacting upper states: (0 2 0), (1 0 0), and (0 0 1). J Mol Spectrosc 1999;194:28–42.
[21] Toth RA. The $2v_2 - v_2$ and $2v_2$ bands of $H_2^{16}O$, $H_2^{17}O$, and $H_2^{18}O$: line positions and strengths. J Opt Soc Am B 1993;B10:1526–44.
[22] Toth RA. The v_1 and v_3 bands of $H_2^{17}O$ and $H_2^{18}O$: line positions and strengths. J Mol Spectrosc 1994;166:184–203.
[23] Toth RA, Brown LR, Plymate C. Self-broadened widths and frequency shifts of water vapor lines between 590 and 2400 cm^{-1}. JQSRT 1998;59:529–62.
[24] Toth RA. Air- and N_2-broadening parameters of water vapor: 604 to 2271 cm^{-1}. J Mol Spectrosc 2000;201:218–43.
[25] Toth RA. Air- and N_2-broadening parameters of HDO and D_2O, 709 to 1936 cm^{-1}. J Mol Spectrosc 1999;198:358–70.
[26] Rothman LS, Gamache RR, Tipping RH, Rinsland CP, Smith MAH, Chris Benner D, Malathy Devi V, Flaud J-M, Camy-Peyret C, Perrin A, Goldman A, Massie ST, Brown LR, Toth RA. The HITRAN molecular database: editions of 1991 and 1992. JQSRT 1992;48:537–66.
[27] Rothman LS, Rinsland CP, Goldman A, Massie ST, Edwards DP, Flaud J-M, Perrin A, Camy-Peyret C, Dana V, Mandin JY, Schroeder J, Mc Cann A, Gamache RR, Wattson RB, Yoshino K, Chance K, Jucks K, Brown LR, Nemtchinov V, Varanasi P. The HITRAN Molecular Spectroscopic Database and HAWKS (HITRAN Atmospheric Workstation): 1996 edition. JQSRT 1998;60:665–710.
[28] Tashkun SA, Perevalov VI, Teffo J-L, Rothman LS, Tyuterev VlG. Global fitting of $^{12}C^{16}O_2$ vibrational–rotational line positions using the effective Hamiltonian approach. JQSRT 1998;60:785–801.
[29] Tashkun SA, Perevalov VI, Teffo J-L, Tyuterev VlG. Global fit of $^{12}C^{16}O_2$ vibrational–rotational line intensities using the effective operator approach. JQSRT 1999;62:571–98.
[30] Tashkun SA, Perevalov VI, Teffo J-L, Lecoutre M, Huet TR, Campargue A, Bailly D, Esplin MP. $^{13}C^{16}O_2$: Global treatment of vibrational–rotational spectra and first observation of the $2v_1 + 5v_3$ and $v_1 + 2v_2 + 5v_3$ absorption bands. J Mol Spectrosc 2000;200:162–76.
[31] Tashkun SA, Perevalov VI, Teffo J-L. Global fittings of the vibrational–rotational line positions of the $^{16}O^{12}C^{17}O$ and $^{16}O^{12}C^{18}O$ isotopic species of carbon dioxide. J Mol Spectrosc 2001;210:137–45.
[32] Teffo J-L, Daumont L, Claveau C, Valentin A, Tashkun SA, Perevalov VI. Infrared spectra of the $^{16}O^{12}C^{17}O$ and $^{16}O^{12}C^{18}O$ species of carbon dioxide: the region 500–1500 cm^{-1}. J Mol Spectrosc 2002;213:145–52.
[33] Teffo J-L, Daumont L, Claveau C, Valentin A, Tashkun SA, Perevalov VI. Infrared spectra of the $^{16}O^{12}C^{17}O$ and $^{16}O^{12}C^{18}O$ species of carbon dioxide: II. The region 1500–3000 cm^{-1}. J Mol Spectrosc 2003;219:271–81.

[34] Schreier F, Schimpf B, Birk M. FitMAS. Least-squares fitting of molecular line parameters from high resolution Fourier transform spectra. Paper presented at 13th colloquium on high resolution molecular spectroscopy 13–17 September 1993, Univ. degli Studi di Bologna, Riccione, Italy.
[35] Wagner G, Birk M, Schreier F, Flaud J-M. Spectroscopic database for ozone in the fundamental spectral region. J Geophys Res 2002;107(D22):4626–43.
[36] Flaud J-M, Camy-Peyret C, Rinsland CP, Smith MAH, Malathy Devi V. Atlas of ozone spectral parameters from microwave to medium infrared. CA, San Diego: Academic; 1990.
[37] Rinsland CP, Smith MAH, Flaud J-M, Camy-Peyret C, Malathy Devi V. Line positions and intensities of the $2\nu_3$, $\nu_1+\nu_3$ and $2\nu_1$ bands of $^{16}O_3$. J Mol Spectrosc 1988;130:204–12.
[38] Flaud J-M, Camy-Peyret C, Malathy Devi V, Rinsland CP, Smith MAH. The ν_1 and ν_3 bands of $^{16}O^{18}O^{16}O$: line positions and intensities. J Mol Spectrosc 1986;118:334–44.
[39] Flaud J-M, Bacis R. The ozone molecule: infrared and microwave spectroscopy. Spectrochim Acta Part A 1998;54:3–16.
[40] Rothman LS, Barbe A, Chris Benner D, Brown LR, Camy-Peyret C, Carleer MR, Chance K, Clerbaux C, Dana V, Malaty Devi VM, Fayt A, Flaud J-M, Gamache RR, Goldman A, Jacquemart D, Jucks KW, Lafferty WJ, Mandin J-Y, Massie ST, Nemtchinov V, Newnham DA, Perrin A, Rinsland CP, Schroeder J, Smith KM, Smith MAH, Tang K, Toth RA, Vander Auwera J, Varanasi P, Yoshino K. The HITRAN molecular spectroscopic database: edition of 2000 including updates through 2001. JQSRT 2003;82:5–44.
[41] Flaud J-M, Wagner G, Birk M, Camy-Peyret C, Claveau C, De Backer-Barilly M-R, Barbe A, Piccolo C. Ozone absorption around 10 μm. J Geophys Res 2003;108(D9):4269.
[42] Claveau C, Camy-Peyret C, Valentin A, Flaud J-M. Absolute intensities of the ν_1 and ν_3 bands of $^{16}O_3$. J Mol Spectrosc 2001;206:115–25.
[43] De Backer-Barilly MR, Barbe A. Absolute intensities of the 10 μm bands of $^{16}O_3$. J Mol Spectrosc 2001;205:43–53.
[44] Smith MAH, Malathy Devi V, Benner DC, Rinsland CP. Absolute intensities of $^{16}O_3$ lines in the 9–11 μm region. J Geophys Res 2001;106:9909–21.
[45] Brown LR, Gunson MR, Irion W, Toth RA, Rinsland CP, Goldman A. The 1995 ATMOS compilation of molecular parameters. Appl Opt 1996;35:2828–48.
[46] Flaud JM, Camy-Peyret C, Rinsland CP, Smith MAH, Malathy-Devi V. Line parameters for $^{16}O_3$ bands in the 7-μm region. J Mol Spectrosc 1989;134:106–12.
[47] Barbe A, Chichery A, Tyuterev VlG, Tashkun S, Mikhailenko S. The $2\nu_2$ and $3\nu_2$–ν_2 bands of ozone. Spectrochim Acta Part A 1998;54:1935–45.
[48] Chichery A, Barbe A, Tyuterev VlG, Sulakshina ON, Borkov Y. Intensities of the difference bands $\nu_1+\nu_3-\nu_2$ and $2\nu_3-\nu_2$ of ozone. Comparison with theoretical predictions. J Mol Struct 2000;517–18:165–70.
[49] De Backer-Barilly MR, Barbe A, Tyuterev VlG. Infrared spectrum of $^{16}O^{18}O^{16}O$ in the 5 μm range: positions, intensities, and atmospheric applications. Atmos Oceanic Opt 2003;16:183–8.
[50] Flaud J-M, Camy-Peyret C, N'Gom A, Malathy Devi V, Rinsland CP, Smith MAH. The ν_2 bands of $^{16}O^{18}O^{16}O$ and $^{16}O^{16}O^{18}O$: line positions and intensities. J Mol Spectrosc 1989;133:217–23.
[51] Mikhailenko S, Barbe A, Tyuterev VlG. Extended analysis of line positions and intensities of ozone bands in the 2900–3400 cm^{-1} region. J Mol Spectrosc 2002;215:29–41.
[52] Flaud J-M, Camy-Peyret C, Malathy Devi V, Rinsland CP, Smith MAH. The ν_1 and ν_3 bands of $^{16}O_3$: line positions and intensities. J Mol Spectrosc 1987;124:209–17.
[53] Barbe A, Plateaux JJ, Bouazza S, Sulakshina ON, Mikhailenko SN, Tyuterev VlG, Tashkun SA. Experimental and theoretical study of absolute intensities of ozone spectral lines in the range 1850–2300 cm^{-1}. JQSRT 1994;52:341–55.
[54] Barbe A, Sulakshina ON, Plateaux JJ, Hamdouni A, Bouazza S. High-resolution infrared spectra of ozone in the 2300–2600 cm^{-1} region. J Mol Spectrosc 1995;170:244–50.
[55] Malathy Devi V, Flaud J-M, Camy-Peyret C, Rinsland CP, Smith MAH. Line positions and intensities for the $\nu_1+\nu_2$ and $\nu_2+\nu_3$ bands of $^{16}O_3$. J Mol Spectrosc 1987;125:174–83.
[56] Toth RA. Frequencies of N_2O in the 1100- to 1440 cm^{-1} region. J Opt Soc Am B 1986;3:1263–81.
[57] Toth RA. Line strengths of N_2O in the 1120–1440 cm^{-1} region. Appl Opt 1984;23:1825–34.

[58] Toth RA. Line strengths (900–3600 cm^{-1}), self-broadened line widths, and frequency shifts (1800–2360 cm^{-1}) of N_2O. Appl Opt 1993;32:7326–65.
[59] Lyulin OM, Perevalov VI, Teffo J-L. Effective dipole moment and band intensities of nitrous oxide. J Mol Spectrosc 1995;174:566–80.
[60] Daumont L, Claveau C, Debacker-Barilly MR, Hamdouni A, Régalia-Jarlot L, Teffo J-L, Tashkun S, Perevalov VI. Line intensities of $^{14}N_2^{16}O$: the 10 micrometers region revisited. JQSRT 2002;72:37–55.
[61] Brown LR, Benner DC, Champion J-P, Malathy Devi VM, Fejard L, Gamache RR, Gabard T, Hilico JC, Lavorel B, Loete M, Mellau GCh, Nikitin A, Pine AS, Predoi-Cross A, Rinsland CP, Robert O, Sams RL, Smith MAH, Tashkun SA, Tyuterev VlG. Methane line parameters in HITRAN. JQSRT 2003;82:219–38.
[62] Champion J-P, Hilico JC, Wenger C, Brown LR. Analysis of the v_2/v_4 Dyad of $^{12}CH_4$ and $^{13}CH_4$. J Mol Spectrosc 1989;133:256–72.
[63] Brown LR, Loete M, Hilico JC. Line strengths of the v_2 and v_4 bands of $^{12}CH_4$ and $^{13}CH_4$. J Mol Spectrosc 1989;133:273–311.
[64] Ouardi O, Hilico JC, Loete M, Brown LR. The hot bands of methane between 5 and 10 μm. J Mol Spectrosc 1996;180:311–22.
[65] Nikitin A, Champion J-P, Tyuterev VlG. Improved algorithms for the modeling of vibrational polyads of polyatomic molecules: application to T_d, O_h, and C_{3v} molecules. J Mol Spectrosc 1998;182:72–84.
[66] Nikitin A, Champion J-P, Tyuterev VlG. The MIRS computer package for the modeling of vibration–rotation spectra of polyatomic molecules. JQSRT 2003;82:239–49.
[67] Nikitin A, Champion J-P, Tyuterev VlG, Brown LR. The high resolution infrared spectrum of CH_3D in the region 900–1700 cm^{-1}. J Mol Spectrosc 1997;184:120–8.
[68] Nikitin A, Champion J-P, Tyuterev VlG, Brown LR, Mellau G, Lock M. The infrared spectrum of CH_3D between 900 and 3200 cm^{-1}: extended assignment and modeling. J Mol Struct 2000;517:1–24.
[69] Brown LR, Nikitin A, Malathy Devi VM, Benner DC, Smith MAH, Fejard L, Champion J-P, Tyuterev VlG. Line intensities of CH_3D in the triad region: 6–10 μm. J Mol Struct 2004; 695–696:181–88.
[70] Hilico JC, Champion J-P, Toumi S, Tyuterev VlG, Tashkun SA. New analysis of the pentad system of methane and prediction of the (pentad–pentad) spectrum. J Mol Spectrosc 1994;168:455–76.
[71] Fejard L, Champion J-P, Jouvard JM, Brown LR, Pine AS. The intensities of methane in the 3–5 μm region revisited. J Mol Spectrosc 2000;201:83–94.
[72] Jouvard JM, Lavorel B, Champion J-P, Brown LR. Preliminary analysis of the pentad of $^{13}CH_4$ from Raman and infrared spectra. J Mol Spectrosc 1991;150:201–17.
[73] Nikitin A, Brown LR, Fejard L, Champion J-P, Tyuterev VlG. Analysis of the CH_3D nonad from 2000–3300 cm^{-1}. J Mol Spectrosc 2002;216:225–51.
[74] Hilico JC, Baronov GS, Bronnikov DK, Gavrikov SA, Nikolaev II, Rusanov VD, Filimonov YG. High-resolution spectroscopy of (pentad–dyad) and (octad–pentad) hot bands of methane in a supersonic jet. J Mol Spectrosc 1993;161:435–44.
[75] Brown LR, Margolis JS, Champion J-P, Hilico JC, Jouvard JM, Loete M, Chackerian C, Tarrago G, Benner DC. Methane and its isotopes—current status and prospects for improvement. JQSRT 1992;48:617–28.
[76] Smith MAH, Rinsland CP, Malathy Devi VM, Benner DC. Temperature-dependence of broadening and shifts of methane lines in the v_4 band. Spectrochim Acta 1992;48A:257–72.
[77] Malathy Devi VM, Benner DC, H Smith MA, Rinsland CP. Temperature-dependence of Lorentz air-broadening and pressure-shift coefficients of $^{12}CH_4$ lines in the 2.3-μm spectral region. JQSRT 1994;51:439–65.
[78] Chackerian Jr C, Freedman RS, Giver LP, Brown LR. The NO vibrational fundamental band: O_2-broadening coefficients. J Mol Spectrosc 1998;192:215–9.
[79] Spencer MN, Chackerian Jr C, Giver LP, Brown LR. The nitric oxide fundamental band: frequency and shape parameters for ro-vibrational lines. J Mol Spectrosc 1994;165:506–24.
[80] Goldman A. Private communication; 2003.
[81] Mandin J-Y, Dana V, Perrin A, Flaud J-M, Camy-Peyret C, Régalia L, Barbe A. The $\{v_1+2v_2, v_1+v_3\}$ bands of $^{14}N^{16}O_2$: line positions and intensities; line intensities in the $v_1+v_2+v_3-v_2$ hot band. J Mol Spectrosc 1997;181:379–88.

[82] Dana V, Mandin J-Y, Allout M-Y, Perrin A, Régalia L, Barbe A, Plateaux J-J, Thomas X. Broadening parameters of NO_2 lines in the 3.4 μm spectral region. JQSRT 1997;57:445–58.
[83] Malathy Devi V, Fridovich B, Jones GD, Snyder DGS, Das PP, Flaud J-M, Camy-Peyret C, Narahari Rao K. Tunable diode laser spectroscopy of NO_2 at 6.2 μm. J Mol Spectrosc 1982;93:179–95.
[84] Malathy Devi V, Fridovich B, Jones GD, Snyder DGS, Neuendorffer A. Temperature dependence of the widths of N_2-broadened lines of the v_3 band of $^{14}N^{16}O_2$. Appl Opt 1982;21:1537–8.
[85] May RD, Webster CR. Laboratory measurements of NO_2 line parameters near 1600 cm^{-1} for the interpretation of stratospheric spectra. Geophys Res Lett 1990;17:2157–60.
[86] Perrin A, Flaud J-M, Camy-Peyret C, Hurtmans D, Herman M, Guelachvili G. The $v_2 + v_3$ and $v_2 + v_3 - v_2$ bands of $^{14}N^{16}O_2$: line positions and intensities. J Mol Spectrosc 1994;168:54–66.
[87] Mandin J-Y, Dana V, Claveau C. Line intensities in the v_5 band of acetylene $^{12}C_2H_2$. JQSRT 2000;67:429–46.
[88] Jacquemart D, Claveau C, Mandin J-Y, Dana V. Line intensities of hot bands in the 13.6 μm spectral region of acetylene $^{12}C_2H_2$. JQSRT 2001;69:81–101.
[89] Jacquemart D, Mandin J-Y, Dana V, Régalia-Jarlot L, Thomas X, Von Der Heyden P. Multispectrum fitting measurements of line parameters for 5 μm cold bands of acetylene. JQSRT 2002;75:397–422.
[90] Jacquemart D, Mandin J-Y, Dana V, Régalia-Jarlot L, Plateaux J-J, Décatoire D, Rothman LS. The spectrum of acetylene in the 5 μm region from new line parameter measurements. JQSRT 2003;76:237–67.
[91] Vander Auwera J. Absolute intensities measurements in the $v_4 + v_5$ band of $^{12}C_2H_2$: Analysis of Herman–Wallis effects and forbidden transitions. J Mol Spectrosc 2000;201:143–50.
[92] Kabbadj Y, Herman M, Di Lonardo G, Fusina L, Johns JWC. The bending energy levels of C_2H_2. J Mol Spectrosc 1991;150:535–65.
[93] Lambot D, Blanquet G, Bouanich J-P. Diode laser measurements of collisional broadening in the v_5 band of C_2H_2 perturbed by O_2 and N_2. J Mol Spectrosc 1989;136:86–92.
[94] Bouanich J-P, Lambot D, Blanquet G, Walrand J. N_2- and O_2-broadening coefficients of C_2H_2 IR lines. J Mol Spectrosc 1990;140:195–213.
[95] Bouanich J-P, Blanquet G, Populaire J-C, Walrand J. Nitrogen broadening of acetylene lines in the v_5 band at low temperature. J Mol Spectrosc 1998;190:7–14.
[96] Babay A, Ibrahimi M, Lemaire V, Lemoine B, Rohart F, Bouanich J-P. Line frequency shifting in the v_5 band of C_2H_2. JQSRT 1998;59:195–202.
[97] Bouanich J-P, Blanquet G, Walrand J. Oxygen broadening of acetylene lines in the v_5 band at low temperature. J Mol Spectrosc 1999;194:269–77.
[98] Hurley MD. Private communication; 2003.
[99] Christidis N, Hurley MD, Pinnock S, Shine KP, Wallington TJ. Radiative forcing of climate change by CFC-11 and possible CFC replacements. J Geophys Res 1997;102:19597–609.
[100] Heathfield AE, Anastasi A, McCulloch A, Nicolaisen FM. Integrated infrared absorption coefficients of several partially fluorinated ether compounds: $CF_3OCF_2H, CF_2HOCF_2H, CH_3OCF_2CF_2H, CH_3OCF_2CFClH, CH_3CH_2OCF_2CF_2H, CF_3CH_2OCF_2CF_2H$ and $CH_2 = CHCH_2OCF_2CF_2H$. JQSRT 1998;32:2825–33.
[101] Smith KP. Private communication; 2003.
[102] Li Z, Varanasi P. Measurement of the absorption cross-sections of CFC-11 at conditions representing various model atmospheres. JQSRT 1994;52:137–44.
[103] Varanasi P. Private communication; 2000.
[104] Clerbaux C, Colin R, Simon PC, Granier C. Infrared cross sections and global warming potentials of 10 alternative hydrohalocarbons. J Geophys Res 1993;98:10491–7.
[105] Varanasi P, Nemtchinov V. Thermal infrared absorption coefficients of CFC-12 at atmospheric conditions. JQSRT 1994;51:679–87.
[106] Nemtchinov V, Varanasi P. Thermal infrared absorption cross- of CF_4 for atmospheric applications. JQSRT 2003;82:461–71.
[107] Vander Auwera J. Private communication; 2003.
[108] Ballard J, Knight RJ, Newnham DA, Vander Auwera J, Herman M, Di Lonardo G, Masciarelli G, Nicolaisen FM, Beukes JA, Christensen LK, McPheat R, Duxbury G, Freckleton R, Shine KP. An intercomparison of

laboratory measurements of absorption cross-sections and integrated absorption intensities for HCFC-22. JQSRT 2000;66:109–28.
[109] Pinnock S, Hurley MD, Shine KP, Wallington TJ, Smyth TJ. Radiative forcing of climate by hydrochlorofluorocarbons and hydrofluorocarbons. J Geophys Res 1995;100:23227–38.
[110] Varanasi P. Private communication; 2001.
[111] Varanasi P. Absorption spectra of HCFC-22 around 829 cm^{-1} at atmospheric conditions. JQSRT 1992;47:251–5.
[112] Varanasi P, Nemtchinov V, Li Z, Cherukuri A. Spectral absorption-coefficient data on HCFC-22 and SF_6 for remote sensing applications. JQSRT 1994;52:323–32.
[113] Wagner G, Birk M. Private communication; 2003.
[114] Wagner G, Birk M. New infrared spectroscopic database for chlorine nitrate. JQSRT 2003;82:443–60.
[115] Nemtchinov V, Varanasi P. Thermal infrared absorption cross-sections of CCl_4 needed for atmospheric remote-sensing. JQSRT 2003;82:473–81.
[116] Chédin A, Scott NA, Wahiche C, Moulinier P. Improved initialization inversion method: a high resolution physical method for temperature retrievals from the TIROS-N series. J Climate Appl Meteorol 1985;24:124–43.
[117] Chevallier F, Chéruy F, Scott NA, Chédin A. A neural network approach for a fast and accurate computation of a longwave radiation budget. J Appl Meteorol 1998;37:1385–97.
[118] Massie ST. Private communication; 2000.
[119] Massie ST. Indices of refraction for the HITRAN compilation. JQSRT 1994;52:501–13.
[120] Massie ST, Goldman A. The infrared absorption cross section and refractive-index data in HITRAN. JQSRT 2003;82:413–28.
[121] Rublev AA. Algorithm and computation of aerosol phase functions. (Moscow, Russia: Internal Note IAE-5715/16 of Russian Research Center Kurchatov Institute); 1994.
[122] Hess M, Köpke P, Schult I. Optical properties of aerosols and clouds: the software package OPAC. BAMS 1998;79:831–44.
[123] Köpke P, Hess M, Schult I, Shettle EP. Global aerosol dataset. Max-Planck-Institut für Meteorologie. Report No. 243, Hamburg, Germany; 1997.
[124] Norman ML, Miller RE, Worsnop DR. Ternary $H_2SO_4/HNO_3/H_2O$ optical constants: new measurements from aerosol spectroscopy under stratospheric conditions. J Phys Chem 2002;106:6075–83.